On the fabric and state parameters of active clays for contaminant control

Paramètres d'état et concernant le tissu des argiles actives pour le contrôle des contaminants

Mario Manassero
Department of Structural, Geotechnical and Building Engineering, Politecnico di Torino, Italy, mario.manassero@polito.it

ABSTRACT: The osmotic, hydraulic and self-healing efficiency of bentonite-based barriers for the containment of subsoil pollutants is governed not only by the intrinsic chemico-physical parameters of the bentonite, i.e. the solid phase density (ρ_{sk}), the total specific surface (S) and the fixed negative electric surface charge (σ), but also by the chemico-mechanical state parameters that are able to quantify the bulk density and the fabric or texture of the solid skeleton, such as the micro (e_m) and nano (e_n) void ratio, the average number of platelets or lamellae per tactoid ($N_{l,AV}$), the effective solid electric charge concentration ($\overline{c}_{sk0}$) and the Stern layer with reference to its thickness (d_{Stern}) and fraction (f_{Stern}). In turn, the state parameters seem to be controlled by the effective stress history (SH), the ionic electrochemical valence (z_i) and the related exposure sequence of the different salt concentrations (c_s) in the pore solution. A theoretical framework has been set up that is able to describe the chemical, hydraulic and mechanical behavior of bentonites in the case of one-dimensional strain and flow fields. In particular, the relationships between the aforementioned state and intrinsic parameters of a given bentonite with its hydraulic conductivity (k), effective diffusion coefficient (D^*_s), chemico-osmotic efficiency coefficient (ω) and osmotic swelling pressure (u_{sw}) under different stress-histories and solute concentration sequences, are dealt with. The proposed theoretical hydro-chemico-mechanical framework has been validated through a comparison with both the direct measurements of the arrangement of bentonite fabric, through advanced Nuclear Magnetic Resonance (NMR), X-ray diffraction, Small Angle X-ray Spectrometry (SAXS) and Transmission Electron Microscopy (TEM) tests, which have recently become available in the specialized literature, and through indirect assessments, by the interpretation of experimental results from hydraulic conductivity, osmotic swelling pressure, osmotic efficiency, and anion available porosity tests.

RÉSUMÉ: L'efficacité osmotique, hydraulique et auto-cicatrisante des barrières à base de bentonite pour le confinement des polluants du sous-sol est non seulement régie par les paramètres chimico-physiques intrinsèques de la bentonite, tels que la densité de la phase solide (ρ_{sk}), la surface spécifique totale (S) et la charge de surface fixe électrique négative (σ), mais aussi par les paramètres d'état chimico-mécaniques, capables d'identifier la densité apparente et le tissu ou la texture du squelette solide, tels que l'indice de vides a l'échelle micro (e_m) et nano (e_n), le nombre moyen de plaquettes ou lamelles par tactoide ($N_{l,AV}$), la concentration effective de la charge électrique du solide ($\overline{c}_{sk0}$) et la couche de Stern par rapport à son épaisseur (d_{Stern}) et à sa fraction (f_{Stern}). À leur tour, les paramètres d'état semblent être contrôlés par l'histoire des contraintes efficaces (SH), la valence ionique (z_i) et la séquence d'exposition des différentes concentrations de sel (c_s) dans la solution interstitielle. Un cadre théorique, capable de décrire le comportement chimique, hydraulique et mécanique des bentonites dans le cas des déformations unidimensionnelles et des champs d'écoulement, a été mis en place. En particulier, on va présenter les relations entre les paramètres d'état mentionnés ci-dessus et les paramètres intrinsèques d'une bentonite, et sa conductivité hydraulique (k), son coefficient de diffusion effectif (D^*_s), son coefficient d'efficacité osmotique (ω) et sa pression de gonflement (u_{sw}), sous différentes histoires des contraintes et séquences de concentration en soluté. Le cadre hydro-chimico-mécanique théorique proposé a été validé par comparaison avec les mesures directes de l'arrangement du tissu de la bentonite par la résonance magnétique nucléaire avancée (RMN), la diffraction des rayons X, la spectrométrie des rayons X de petit angle (SAXS) et la microscopie électronique de transmission (TEM), récemment disponibles dans la littérature spécialisée, et par une évaluation indirecte en ajustant les résultats expérimentaux de la conductivité hydraulique, de la pression de gonflement, de l'efficacité osmotique et de porosité disponible pour l'anion.

KEYWORDS: smectite fabric, chemo-hydro-mechanical behaviour, constitutive laws, geosynthetic clay liner, nuclear waste disposal

1 INTRODUCTION

Environmental Geotechnics deals with a large variety of applications, such as the characterization of polluted sites and landfill waste, the design of containment systems for subsoil pollutant control, radioactive waste disposal, geo-energy exploitation and bacteria-driven soil modification, among others. Nevertheless, the design of subsoil pollutant containment systems and the risk assessment associated with groundwater contamination from clay lined landfills or the release of contaminants from canisters containing nuclear waste can be considered among the leading streams of Environmental Geotechnics activities from both fundamental research and related practical applications.

Many public institutions and private companies, worldwide, are currently investigating and assessing clayey media, such as bentonites, manmade compacted natural and/or amended clays and natural shales, for their possible use as engineered barriers for waste containment systems and/or as host rocks of geologic repositories for High Level Radioactive Waste (HLRW) (Andra, 2005; Delay et al., 2007; Altmann, 2008; Guyonnet et al., 2009; Bock et al., 2010; SKB, 2011; Altmann et al., 2012; Shackelford and Moore, 2013).

Thanks to their very promising performances (under certain conditions), low volume needs, fully sustainable environmental impacts, high flexibility and low costs, industrially produced sodium bentonites seem to represent the most favourable material for subsoil pollutant control since they are currently and frequently used within both the manufactured geosynthetic clay liners (GCLs) for landfill lining and capping systems and as a buffer material around canisters hosting HLRW within underground repositories at great depth. Nevertheless, sodium

bentonite is considered a highly sensitive material since its long-term performance is influenced to a great extent by several factors including physical, chemical and mechanical intrinsic and state parameters involving surface electrical charge, solid skeleton fabric and related void volumes and ionic strength of pore fluids.

When bentonite is employed as filling material within GCLs, its working conditions usually implies low to medium values in terms of both density (void ratio, e = 2 to 5) and effective confining stress (σ' = 10 kPa to 1000 kPa). Within these ranges of the typical physical and mechanical state parameters, both hydraulic conductivity (k) and diffusivity (D^*_s) can play significant roles in terms of pollutant transport. Moreover, other factors, such as the coupled fluxes of solvents and solutes, can greatly influence the barrier performance (Mitchell and Soga, 2005).

In contrast, the conditions that generally exist at great depths where HLRW repositories are located, include very high densities (i.e., e = 0.2 to 1.0) and effective confining stress (σ' = 1000 kPa to 10000 kPa). Under these conditions, bentonite-based barriers (e.g. buffers around canisters hosting HLRW) are characterized by negligible hydraulic conductivities, the ability to self-heal when fractured, and water and solute mass fluxes dominated by molecular diffusion on time-scales (Leroy et al., 2006).

Within the previous considerations, the objectives of the present paper are: 1) to identify and quantify the physical, chemical and mechanical, intrinsic and state parameters that govern the performances (i.e. hydraulic conductivity, diffusivity, osmotic efficiency and osmotic swelling pressure) of bentonites when used as barriers for pollutant control; 2) to link the aforementioned parameters within a theoretical model obtained by upscaling the modified Navier-Stokes and the Nernst-Planck equations and by using the Donnan integration and the imposition of the chemical equilibrium between the bulk electrolyte solution and the internal micro-pore solution; (3) to illustrate the use of the model to simulate the coupled fluxes of ions and water and the influence, on bentonite stress-strain behaviour, of the external actions in terms of both effective stress, pore pressure and electrolyte concentration variations through a modified effective stress principle (Terzaghi, 1936), and last but not least, (4) to establish a relationship within the 3D domain linking electrolyte concentration (c_s), void ratio (e) and the average number of lamellae per tactoid (N_{LAV}) with the latter being a newly introduced fundamental state parameter able to describe and quantify the fabric or texture or structure of bentonite.

The model is potentially able to simulate bentonite performances in terms of clay fabric, throughout the average number of platelets or lamellae per tactoid, N_{LAV}, hydraulic conductivity, k, effective diffusion coefficient, D^*_s, osmotic efficiency, ω, osmotic swelling pressure, u_{sw}, once the intrinsic input parameters, i.e. the solid phase density, ρ_{sk}, the fixed negative electric surface charge, σ, and the total specific surface, S, have been introduced and the input state parameters, i.e. the Stern's layer thickness, d_{Stern}, and the related fraction coefficient, f_{Stern}, the average half distance between the platelets in the tactoid, b_n, the electrolyte concentration in the external solution, c_s, the ions electrochemical valence, z_i, and the void ratio, e, have been assessed and/or imposed.

Lastly, the proposed model has been validated though the comparison with the measurements of bentonite fabric arrangement by advanced techniques such as Nuclear Magnetic Resonance (NMR), X-ray diffraction, Small Angle X-ray Spectrometry (SAXS) and Transmission Electron Microscopy (TEM), that were recently made available within the specialized literature. Moreover, further comparisons have been carried out through the assessment of bentonite fabric arrangement by the theoretical interpretation of experimental results from more traditional techniques such as hydraulic conductivity, osmotic swelling pressure, osmotic efficiency, and anion available pore volume tests, some of which have been conducted originally. For the sake of simplicity, in the following of the paper the two groups of aforementioned experimental techniques are indicated as "direct methods" and "indirect methods", respectively.

2 BENTONITE COMPONENTS AND FABRIC

Bentonite is a clayey soil that usually contains a significant percentage (e.g.>60%) of the high swelling smectite clay mineral, typically montmorillonite, with a 2:1 clay mineral structure comprising two tetrahedral sheets of silica that sandwich a central octahedral sheet of alumina (TOT). A more detailed description of the nature of the mineralogy and fabric of bentonite follows.

2 .1 *Smectite lamellae*

The formula of ideal smectite unit cell is $\{(OH)_4Si_8Al_{3.44}Mg_{0.66}O_{20}\cdot nH_2O^{0.66-}\}$, where n is the number of H_2O interlayered between the (TOT) layers. However, smectite always differs from this ideal formula because of isomorphic substitution of Si^{4+} by Al^{3+} in the silica tetrahedra and Al^{3+} by Fe^{2+} and/or Mg^{2+} in the octahedral layer of the crystal lattice. Most of the isomorphic substitutions occur in the octahedral (gibbsite) sheet, whereas the substitution of Si^{4+} by Al^{3+} in the silica tetrahedra appears to be limited to less than about 15%. Grim (1962) notes that the substitutions in the smectite lattice always result in about 0.66 net negative charge per unit cell.

Smectite crystals are organized in terms of parallel-aligned alumino-silicate lamellae, which are approximately 1 nm thick and 100-200 nm in the lateral extent. The unit cell parameters are 0.517 nm and 0.895 nm, which correspond to a unit cell area of 0.925 nm^2, or one unit charge per 1.4 nm^2. The corresponding surface charge, σ, is equal to 0.114 $C\cdot m^{-2}$. The total specific surface of a single platelet, S, available for water adsorption is approximately equal to 760 $m^2\cdot g^{-1}$, assuming a solid density, ρ_{sk}, of 2.65 $Mg\cdot m^{-3}$ corresponding to a specific gravity of solids, G_s, of 2.65 (-).

Smectite particles can be represented as infinitely extended platy particles, also called platelets or lamellae. Norrish (1954) showed that bentonite can have a dispersed structure or fabric in which clay particles are present as well separated units, or an aggregated structure that consists of packets of particles, or tactoids, within which several clay platelets are in a parallel array, with a characteristic interparticle distance of about 0.9 nm (Figure 1).

2 .2 *Tactoid formation and bentonite fabric*

The formation of tactoids has the net result of reducing the surface area of the montmorillonite, which then behaves as a much larger particle with the diffuse double layer fully manifesting itself on only the outside surfaces. The formation of tactoids is due to internal flocculation of the clay platelets, and depends primarily on the concentration and the valence of the ions in the salt solution and, to a lesser extent, on the effective isotropic stress history or, in turn, the total void ratio, e. The average number of clay platelets or lamellae forming tactoids, N_{LAV}, increases with an increase in the ion concentration and valence of cations in the salt solution. However, experimental evidence indicates no apparent unique trend in N_{LAV} versus the total void ratio e for a given concentration.

Referring to the parallel platelet array scheme (figure 1a), the average half distance, b, in perfectly dispersed bentonites, may be estimated (Dominijanni and Manassero, 2012b) from the following relation:

$$b = \frac{e}{\rho_{sk} S} \quad (1)$$

If the clay has an aggregated fabric or structure (Figure 1b), then only the external surface of the tactoids can be assumed to interact with the mobile portion of the pore fluid and related ions in solution.

Therefore, if $N_{l,AV}$ is the average number of platelets per tactoid, the external or effective specific surface, S_{eff}, and the internal specific surface, S_n, are given as follows:

$$S_{eff} = \frac{S}{N_{l,AV}} \quad (2a)$$

$$S_n = S - S_{eff} = \frac{(N_{l,AV} - 1)}{N_{l,AV}} S \quad (2b)$$

Considering the previous scheme, with reference to the effective volume of the conducting pores (Dominijanni et. al., 2017), the thickness of the Stern layers, d_{Stern}, ranging between 1.2 nm and 2.0 nm and consisting of the first row of hydrated cations in direct contact with the negatively charged surface of the solid particles, can be taken into account. The hydrated cations of the Stern layer are characterized by a significantly reduced mobility (Tournassat et al., 2009; Muurinen et al., 2013; Shackelford and Moore, 2013; Tinnacher et al., 2016) and, therefore, can be considered as a part of the solid phase with a consequent restriction of the micro void space directly involved by the solvent and solute fluxes.

Based on the previous assumptions and considerations, the void space within the platelets of the tactoids, together with the thickness of the hydrated cations in the Stern layer surrounding the external surface of the tactoid, should be subtracted from the total void space, e, to obtain the micro-void space, e_m, where almost the entire solute and solvent flow takes place.

The average half distance between the platelets in the tactoid, b_n, as determined by means of X-ray measurements, can vary between 0.2 nm and 0.5 nm (Shainberg et al., 1971; Laird, 2006). In summary, it is possible to assume that the total void ratio, e, of the bentonite is given by the sum of the void ratio inside the tactoid, e_n, representing the nano or non-conductive pores (nm size), plus the volume occupied by the thickness of the Stern layers, and the void ratio representing the micro or conductive pores (μm size), e_m. The water inside the tactoids and the Stern layer can be considered as a portion of the solid particles and is excluded from any transport mechanisms.

Therefore, the void ratio associated with the internal surfaces of the tactoid and the hydrated cations of the Stern layer, e_n, can be estimated as follows:

$$e_n = b_n \rho_{sk} \left(S_n + \frac{S \cdot d_d}{N_{l,AV}} \right) \quad (3)$$

where: d_d is the thickness of the Stern layer consisting of hydrated cations wrapping the external surface of the tactoid (d_{Stern}), divided by the average half distance between the platelets in the tactoid (b_n). Finally, the half distance, between the tactoids, in the case of an aggregate microstructure of bentonite, can be estimated from an equation similar to Eq.1, or:

$$b_m = \frac{e_m}{\rho_{sk} S_{eff}} \quad (4)$$

where: e_m (= $e - e_n$) is the void ratio representing the void space between the tactoids.

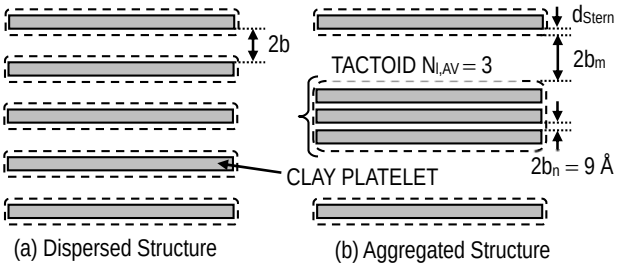

Figure 1. Microscopic structure of clay soils containing montmorillonite as the main mineralogical component. The structure can be dispersed (a), if the lamellae of montmorillonite (or clay platelets) are present as individual units, or aggregated (b), if the lamellae are condensed to form the so-called tactoids. Symbols: $N_{l,AV}$ = number of clay platelets per tactoid; b_m = half distance of the conducting pores; b_n = half distance of the intra-tactoid pores containing immobile water; d_{Stern} = thickness of hydrated cations layer wrapping the external tactoid surface.

For a given total void ratio, e, when $d_d > 1$ and the number of clay platelets in the tactoids, $N_{l,AV}$, increases, the external specific surface decreases and the void ratio, e_m, representing the pore volume available for the solute and solvent transport, increases. In contrast, e_m decreases when $d_d < 1$ and, as in the previous case, $N_{l,AV}$ increases and the external specific surface decreases.

Guyonnet et al. (2005), through a comparison of the results of hydraulic conductivity tests and microscopic analyses of bentonite structure based on small angle X-ray scattering and transmission electron microscopy, showed that high hydraulic conductivity (k) is related to an aggregated fabric (also called the hydrated-solid phase), whereas low k is related to a dispersed fabric (also called the gel phase). These experimental results can be explained by the increase in the average micro-pore size, due to tactoid formation as discussed subsequently in this paper.

3 CHEMICO-MECHANICAL EQUILIBRIUM CONDITIONS

An analysis of chemico-mechanical equilibrium conditions is provided in order to separate partition effects, due to electric interactions between the ions in solutions and montmorillonite particles, from transport mechanisms, related to the motion of the different components of the pore solution. For the sake of simplicity, reference is made to the case of a pore solution containing a single salt, consisting of a cation (e.g. Na^+ or Ca^{2+}) and a common anion (e.g. Cl^-), assumed to be completely dissociated:

$$(\,Cation\,)^{\nu_c}_{z_c} (\,Anion\,)^{\nu_a}_{z_a} \rightarrow \nu_c (\,Cation\,)^{z_c} + \nu_a (\,Anion\,)^{z_a}$$

where (ν_c, z_c) and (ν_a, z_a) are the stoichiometric coefficient and the electrochemical valence of the cation (index c) and the anion (index a), respectively.

The ionic concentrations, c_i ($i = a, c$), in the bulk solution are related to the salt concentration, c_s, as follows:

$$c_i = \nu_i c_s \quad (5)$$

3.1 Equilibrium conditions and partition effect

If a porous medium is placed in contact with an external bulk solution, equilibrium is achieved after a sufficiently long time. At equilibrium and in the absence of partition mechanisms, the

ion concentrations and the hydraulic pressure of the pore solution are equal to the ion concentrations and the hydraulic pressure of the external bulk solution. In contrast, in the presence of partition mechanisms, this equality does not occur and a discontinuity in ion concentrations and hydraulic pressure between the external bulk solution and the pore solution occurs.

In bentonites, the primary partition mechanism is the electrostatic mechanism. At the macroscopic scale, this effect can be taken into account via Donnan's equations that define the equilibrium conditions between the pore solution of a charged porous medium and an external electrolyte solution. Donnan's equations establish the equality of the macroscopic electro-chemical potentials between the components of the pore solution and the components of the external bulk solution, as follows:

$$\overline{\mu}_W = \mu_W \tag{6a}$$

$$\overline{\mu}_i^{ec} = \mu_i^{ec} \text{ ; i = a, c} \tag{6b}$$

where $\overline{\mu}_W$ = chemical potential of water in the pore solution (N·m·mol^{-1}), μ_W = chemical potential of water in the external bulk solution (N·m·mol^{-1}), and $\overline{\mu}_i^{ec}$ = electro-chemical potential of the i-th ion in the pore solution (N·m·mol^{-1}), μ_i^{ec} = electro-chemical potential of the i-th ion in the external bulk solution (N·m·mol^{-1}).

Also, the following definitions of the electro-chemical potentials, valid for dilute solutions, can be used to determine the relations between the pressure and the ion concentrations of the external bulk solution and the pore solution (Katchalsky and Curran, 1965):

$$\begin{aligned} \mu_W &= \mu_W^0 + \frac{1}{c_W}(u - \Pi) \\ \overline{\mu}_W &= \overline{\mu}_W^0 + \frac{1}{\overline{c}_W}(\overline{u} - \overline{\Pi}) \end{aligned} \tag{7a}$$

$$\begin{aligned} \mu_i^{ec} &= \mu_i^0 + RT\ln(c_i) + z_i F\Phi \\ \overline{\mu}_i^{ec} &= \overline{\mu}_i^0 + RT\ln(\overline{c}_i) + z_i F\overline{\Phi} \end{aligned} \tag{7b}$$

where $\mu_b^0, \overline{\mu}_b^0$ (for b = w,a,c) = constants of integration in the external and the pore solution respectively (N·m·mol^{-1}); $c_W, \overline{c}_W$ = water concentration in the external and the pore solution respectively; $u, \overline{u}$ = fluid pressure in the external and the pore solution respectively (Pa); $c_i, \overline{c}_i$ = concentration of the i-th ion in the external and the pore solution respectively (mol/m^3); $\Phi, \overline{\Phi}$ = electric potential in the external and the pore solution respectively (V); $\Pi = RT\sum_{i=1}^{Nions} c_i$ = osmotic pressure in the external solution (Pa); $\overline{\Pi} = RT\sum_{i=1}^{Nions} \overline{c}_i$ = osmotic pressure in the pore solution (Pa); R = universal gas constant (8.314 J·mol^{-1}·K^{-1}); T = absolute temperature (K); and F = Faraday's constant (96,485 C/mol).

Assuming that $\mu_b^0 = \overline{\mu}_b^0$ (for b = w,a,c) and noting that the partition mechanism, based on the electrostatic interaction between the solid particles and the molecules in the pore solutions, acts only on the ion species and not on the electro-neutral water molecules, such that $c_W = \overline{c}_W$, Eqs. 7a,b can be expressed as follows:

$$\overline{u} - \overline{\Pi} = u - \Pi \tag{8}$$

$$\overline{c}_i = c_i \exp\left(-z_i \frac{F}{RT}\Psi\right) \tag{9}$$

where $\Psi = \overline{\Phi} - \Phi$ is the Donnan potential representing the characteristic electric potential of the solid skeleton.

An ion partition coefficient, Γ_i (-), can also be conveniently introduced as follows:

$$\Gamma_i = \frac{\overline{c}_i}{c_i} = \exp\left(-z_i \frac{F}{RT}\Psi\right) \tag{10}$$

In order to close the system, the following equation, expressing the electro-neutrality condition within the pore solution, is required:

$$\sum z_i \overline{c}_i = \frac{\overline{c}_{sk,0}}{e_m} \tag{11}$$

where $\overline{c}_{sk,0}$ = effective solid charge concentration of solid skeleton within pore solution (mol/m^3).

In the case of a solution containing a (1:1) electrolyte (e.g. NaCl or KCl), the ion partition coefficients are given by:

$$\Gamma_a = \Gamma_c^{-1} = -\frac{\xi}{2} + \sqrt{\left(\frac{\xi}{2}\right)^2 + 1} \tag{12}$$

where: $\xi = \dfrac{\overline{c}_{sk,0}}{e_m c_s}$

The coefficient $\Gamma_c \geq 1$ describes the accumulation of the cations within bentonite pores, whereas $0 \leq \Gamma_a \leq 1$ describes the exclusion of the anions. When $\Gamma_c = \Gamma_a = 1$, bentonite does not generate a partition of the ions and has no selective capability. When $\Gamma_a = 0$ and $\Gamma_c \to \infty$ the membrane is "ideal" or "perfect", such that the passage of the salt is completely restricted.

The term $\overline{c}_{sk,0}$ can be estimated on the basis of an idealised model for bentonite fabric. Bentonite can display a hierarchy of structures that are referred as lamellae at the finest level, tactoids or quasi-crystals or particles at the microscopic level, micro-aggregate or cluster at the mesoscopic level and macro-aggregates or peds on the macroscopic scale. A low k(< 10^{-9} m/s) is compatible only with the absence of micro and macro aggregates. If the tactoids are assumed to be formed by packets of parallel lamellae (platelets) such that the only mobile fraction of the pore solution is that located in the inter-tactoids pore space, while the pore solution within the tactoids is considered as part of the solid phase, then $\overline{c}_{sk,0}$ can be estimated as follows (Dominijanni and Manassero, 2008, 2012a, 2012b; Dominijanni et al., 2013):

$$\overline{c}_{sk,0} = \frac{(1 - f_{Stern}) \cdot \sigma \cdot \rho_{sk} \cdot S_{eff}}{F} \tag{13}$$

where, for ease of reading, the following definitions and related units are repeated: f_{Stern} = fraction of electric charge compensated by the cations specifically adsorbed in the Stern layer (-), σ = electric surface charge of lamellae (C/m^2), ρ_{sk} =

density of solid phase (g/m^3), S_{eff} = effective specific surface of tactoids (m^2/g).

3.2 Osmotic swelling pressure

Under the assumption of elastic behaviour of the solid skeleton (no free energy dissipation during the deformation processes) and very small area of the inter-tactoid contacts in comparison with the total area of a generic cross section of the soil (Skempton, 1961), the inter-tactoid stress can be defined directly at the macroscopic scale without having to employ an upscaling procedure, such that the inter-granular or effective stress, σ', for bentonite can be expressed as follows in the case of electrically charged soil surface that is in contact with a single electrolyte solution (Dominijanni and Manassero, 2008):

$$\sigma' = \sigma - \overline{u} = \sigma - u - \underbrace{(\overline{\Pi} - \Pi)}_{u_{sw}} \tag{14}$$

where:

$$u_{sw} = 2RTc_s\left[\sqrt{\left(\frac{\xi}{2}\right)^2 + 1} - 1\right] \tag{15}$$

The term u_{sw}, which is a function of $\overline{c}_{sk,0}$, c_s and e_m through Eqs. 8 and 12, represents the osmotic swelling pressure.

When the salt concentration increases, the osmotic swelling pressure decreases up to negligible values. Thus, higher values of osmotic swelling pressure are associated with higher values of $\overline{c}_{sk,0}$.

At low salt concentrations, the osmotic swelling pressure tends to the theoretical maximum value, given as: $u_{sw} = RT \cdot \overline{c}_{sk,0} / e_m$

Taking the oedometric conditions into consideration and based on the previous assumptions, and more specifically at the volumetric rigidity under the external actions of the tactoids (i.e. $de_n=0$), the micro void ratio, e_m, of the surface charged soil is related to the effective stresses as follows:

$$e_m = e_{m,0} - a_v(\sigma' - \sigma'_0) \tag{16}$$

where: a_v = bentonite compressibility of intergranular contacts (Pa^{-1}); $e_{m,0}$ = void ratio at a reference state (-); and σ'_0 = effective stress at a reference state (1 Pa). Using Eqs. 14 and 15 the void ratio is related, not only to the apparent effective stress σ' ($= \sigma - u$), but also to the chemical composition and ion concentration of the pore solution through the osmotic swelling pressure u_{sw}.

High salt concentration and substitution of di-valent for mono-valent cations result in a reduction of the osmotic swelling pressure and a consequent increase of the effective stress. Such an increase in effective stress results in compression of bentonite, i.e. a reduction of the void ratio, a process referred to as "chemical consolidation" by Kaczmarek and Hueckel (1998).

However local increase of effective stress at the microscopic scale can promote aggregation of montmorillonite lamellae, causing the formation of thicker tactoids. The increase in the number of lamellae per tactoid determines a reduction of S_{eff}, and a possible increase of intergranular contact resulting in a decrease of the compressibility, a_v. Such modifications of bentonite fabric result, at the macroscopic scale, in an enhance of mechanical characteristics, as rigidity and shear strength, and a degradation of barrier properties (i.e. an increase k). This last effect is of particular concern for environmental applications.

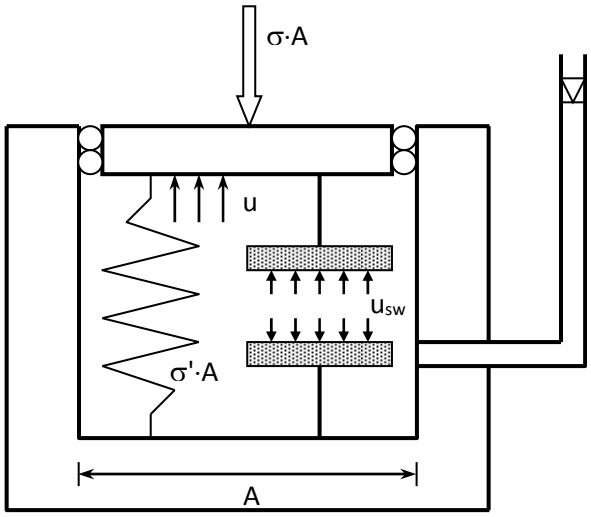

Figure 2. Mechanical model of charged porous medium.

In bentonite characterized by a very high void ratio, as in the case of bentonite suspensions, a lack of contacts between solid particles can be assumed such that effective stresses can be considered nil. Such an assumption has been made, for instance, by Bolt (1956) and is equivalent to assuming $d\sigma' = 0$ or $a_V \to \infty$.

As far as Terzaghi's effective stress principle for soils is concerned, a simple modification is sufficient to model the mechanical behaviour of a charged porous medium, such as bentonite. In fact, the osmotic swelling pressure can be taken into account by a second effect representing the interaction of repulsive forces by the solid particles at the microscopic scale. From Figure 2 and Eq. 14 it is apparent that equilibrium with external forces can also be reached in the absence of the spring representing the intergranular contacts.

An interesting development related to Eq. 16 can be obtained by a differentiation and re-formulation as follows:

$$d\varepsilon_v = \frac{a_v}{1+e_{m,0}} \cdot d\left(\sigma - u - u_{sw}\right) = \frac{-de_m}{1+e_{m,0}} \tag{17}$$

where ε_V represents the volumetric strain.

The development of the stress component differentiations gives:

$$d(\sigma - u - u_{sw}) = d(\sigma - u) - \frac{du_{sw}}{de_m}de_m - \frac{du_{sw}}{d\Pi}d\Pi \tag{18}$$

and, therefore, the micro void ratio variation, de_m, can be expressed as a function of the Terzaghi effective stress, $\sigma' = (\sigma - u)$, the osmotic swelling pressure u_{sw}, the salt concentration c_s and the effective charge concentration on the solid skeleton, $\overline{c}_{sk,0}$ or

$$de = -\frac{a_v a_\pi}{a_v + a_\pi}\left[d(\sigma - u) + \varpi \cdot d\Pi\right] \tag{19}$$

where:

$$\varpi = 1 - \frac{1}{\sqrt{\left(\frac{\xi}{2}\right)^2 + 1}};\quad a_\pi = \frac{2c_s e_m^3\sqrt{\left(\frac{\xi}{2}\right)^2 + 1}}{RT\overline{c}_{sk,0}^2};\quad \Pi = 2RTc_s$$

An interesting observation is that further integration of Eq.19 represents the fundamental Fabric State Surface (FSS) of the chemico-mechanical behaviour of the bentonite (Figures 3a,b,c), since the result links the external salt concentration, c_s, the micro void ratio, e_m and the average number of lamellae per tactoid, $N_{l,AV}$, which is inversely proportional to $\overline{c}_{sk,0}$ which, in turn, is directly linked to the Faraday constant, F, and to the intrinsic parameters including the total surface fixed charge concentration, σ, the total specific surface of the basic lamellae, S, and the solid phase density ρ_{sk}, of the bentonite.

Moreover, the remaining input state parameters to be taken into account, i.e. the average half distance between two platelets in the tactoid, b_n (ranging from 0.8 to 1.0 nm), the Stern fraction, f_{Stern} (ranging from 0.75 to 0.95) and the thickness d_{Stern} (ranging from 1.2 to 2.0 nm) are characterized by a narrow range of variation that can be assessed and used without significant reliability problems for current predictions. In contrast, in the case of interpretation of experimental results these parameters can be used to optimise the final calibration of the model parameters.

The range of validity of Eq. 19 in representing the FSS of the bentonite is limited to micro void size and related distances between tactoids that are significantly greater than the nano void size and related distances between the platelets of the same tactoid. This limitation occurs because, when the dispersed platelets reach the critical distance corresponding to the van der Waals attraction overcoming the electrostatic repulsion, e.g. under exceptionally high confining effective stresses, tactoid formation occurs also in presence of very low electrolyte concentrations such as deionized water (i.e. a solution having a null salt concentration, $c_s = 0$) and this phenomenon is not taken into account by Eq. 19. Thus, the consequent change of e_m versus $N_{l,AV}$ trend, i.e. the increase in the number of lamellae per tactoid when e_m decreases up to $e_m = 0$, cannot be represented by Eq. 19.

Moreover, note that appropriate boundary conditions have been used for getting the best fit, by integration of Eq. 19, of the leading group of experimental results that will be subsequently illustrated. The obtained FSS is shown in Figures 3a,b,c

Unfortunately, the integration of the Eq. 19 is complex and cannot be solved in a closed form. Therefore, as shown subsequently, an approximate solution has been formulated (Figures 3d,e,f) in order to facilitate an efficient use of the proposed model, particularly, with respect to the aforementioned change in the trend of e_m versus $N_{l,AV}$ at extremely high effective confining stresses and correspondingly very small total void ratio (Figure 3d).

4 COUPLED FLUXES AND TRANSPORT

In the case of the most general approach to model the coupled fluxes in porous media, invoking the phenomenological equations, based on the Thermodynamics of Irreversible Processes, is convenient (Katchalsky and Curran, 1965; Yaroshchuk, 1995; Manassero and Dominijanni, 2003). The primary advantage of this approach is to avoid any specification of physical properties of the membrane, maintaining the model to be as general as possible. Using such a formalism, Spiegler and Kedem (1966) derived the following equations for a semipermeable membrane permeated by a solution containing a single salt (e.g. NaCl, KCl or $CaCl_2$):

$$q = -P_{v\lambda}\left(\frac{du}{dx} - \omega_\lambda \frac{d\Pi}{dx}\right) \tag{20}$$

$$J_s = (1-\omega_\lambda)qc_s - P_{s\lambda}\frac{dc_s}{dx} \tag{21}$$

where q = volumetric solution flux ($m^3m^{-2}s^{-1}$), J_s = salt mass flux ($mol \cdot m^{-2}s^{-1}$), and $\Pi = (\nu_a+\nu_c)RTc_s$ = virtual osmotic pressure (N/m^2). In Eqs. 20 and 21, there are three phenomenological coefficients viz.: (1) $P_{v\lambda}$ is the specific hydraulic conductivity ($m^4 \cdot s^{-1} \cdot N^{-1}$), (2) ω_λ is the local chemico-osmotic efficiency coefficient (-), and (3) $P_{s\lambda}$ is the local salt permeability (m^2/s). The state variables are the virtual hydraulic pressure, u, and the virtual salt concentration, c_s, which represent the pressure and the salt concentration of a virtual external bulk solution that is assumed to be in thermodynamic equilibrium with the pore solution in correspondence to a given volume element of the porous medium. Virtual variables can be used to avoid the introduction of any physical assumption on the formulation of flux equations. At the boundaries, the virtual solution coincides with the real bulk solution in contact with the porous medium. Therefore, the steady-state solutions of Eqs. 20 and 21 can be expressed using the pressure and the salt concentration of the bulk solutions in contact with the bentonite barrier as boundary conditions.

Also the phenomenological coefficients $P_{v\lambda}$, ω_λ and $P_{s\lambda}$ are unspecified functions of the salt concentration, c_s, and the hydraulic pressure, u (or the void ratio e_m).

The specific hydraulic conductivity can be expressed in terms of the more common local hydraulic conductivity, k_λ, as follows:

$$P_{v\lambda} = \frac{k_\lambda}{\gamma_w} \tag{22}$$

where γ_w is the water unit weight (N/m^3).

Based on this approach, all the phenomenological coefficients can be measured by means of suitable tests, without any assumption about their relation to physical properties of the bentonite barrier. However, the experimental determination of these parameters is particularly difficult due to their dependency on the salt concentration.

By linearizing the flux equations (Eqs. 20 and 21) an analytical solution at steady-state conditions can be obtained as follows:

$$q = \frac{k}{\gamma_w}\left(\frac{\Delta u}{L} - \omega\frac{\Delta\Pi}{L}\right) \tag{23}$$

$$J_s = (1-\omega)q\frac{c_s' exp(P_{L\pi}) - c_s''}{exp(P_{L\pi}) - 1} \tag{24}$$

where

$$P_{L\pi} = \frac{(1-\omega)qL}{P_s} \tag{25}$$

and L is the length of the barrier, c_s', c_s'' represent the salt concentrations of the external bulk solutions in contact with the barrier at the boundaries and Δu, $\Delta\Pi$ are the differences in hydraulic and osmotic pressure across the porous medium.

In Eqs. 23-25, the global coefficients k, ω, and P_s are average values of the local ones, or:

$$k = \frac{1}{L}\int_0^L k_\lambda \cdot dx \cong \frac{1}{\Delta c_s}\int_{c_s'}^{c_s''} k_\lambda \cdot dc_s \tag{26}$$

$$\omega = \frac{1}{L}\int_0^L \omega_\lambda \cdot dx \cong \frac{1}{\Delta c_s}\int_{c_s'}^{c_s''} \omega_\lambda \cdot dc_s \tag{27}$$

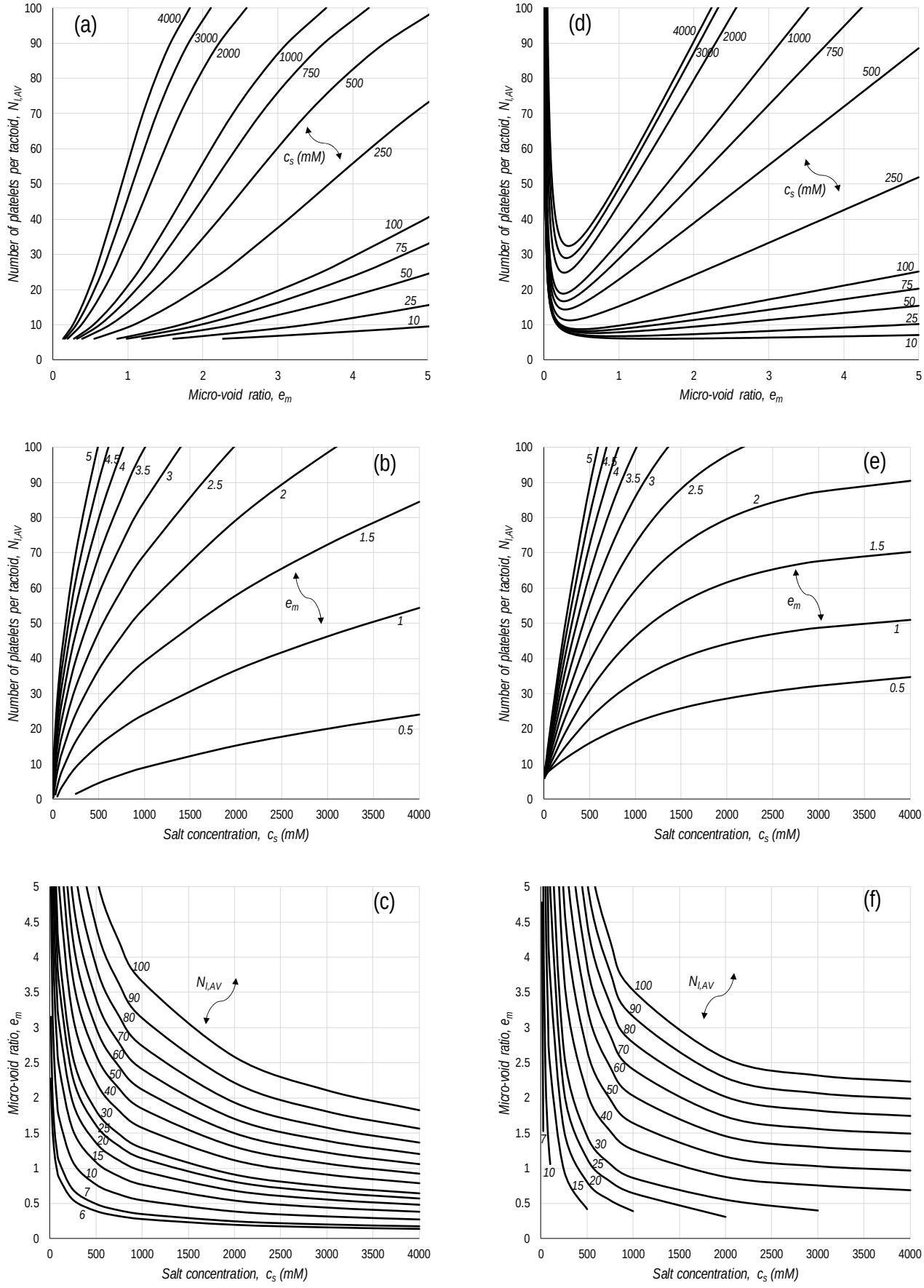

Figure 3. Fabric state surface (FSS): (a)(b)(c) theoretical derivation; (d)(e)(f) operative simplified version.

$$P_s = \frac{1}{L}\int_0^L P_{s\lambda} \cdot dx \cong \frac{1}{\Delta c_s}\int_{c_s'}^{c_s''} P_{s\lambda} \cdot dc_s \qquad (28)$$

where $\Delta c_s = c_s' - c_s''$.

In order to obtain an understanding of the physical meaning of the phenomenological coefficients, although limiting the generality of the approach, Dominijanni and Manassero (2005), Dominijanni et al. (2006), Manassero and Dominijanni (2010) and Manassero et al. (2014) proposed a model obtained by upscaling the modified Navier-Stokes equation and the Nernst-Planck equations and using the Donnan's equations to express the relations between real and virtual variables. The proposed model provides an interpretation of the experimental results of Malusis and Shackelford (2002a,b), Malusis et al. (2013), Dominijanni et al. (2013) and Shackelford et al. (2016).

Based on the theoretical and experimental findings, the following observations were made.

First, the hydraulic conductivity, k_λ, corresponding to relatively low values of the salt concentration ($\leq 10^{-1}$ M), is dependent on the salt concentration due to the electroviscous effect and can be expressed as follows:

$$k_\lambda = \frac{\tau_m}{3}\frac{e_m^3}{(1+e_m)}\frac{\gamma_w}{(\rho_{sk}S_{eff})^2}\frac{1}{\mu_e(c_s', c_s'', \bar{c}_{sk,0})} \qquad (29)$$

where τ_m = matrix tortuosity factor ($\leq$ 1) that takes into account the tortuous nature of the actual migration pathways through the porous medium due to the geometry of the interconnected pores and μ_e = electro-viscous coefficient, which is related to the boundary salt concentrations c_s', c_s'' and the fixed charge concentration, $\bar{c}_{sk,0}$. The τ_m for bentonites can be estimated, as a first approximation, to a range on the order of 0.1 to 0.3 (see Kato et al., 1995; Ichikawa et al., 2004; Bourg et al., 2006)

Moreover, if the electro-viscous effect is neglected, the electro-viscous coefficient can be considered almost equal to the viscous coefficient of water, μ_w, and, as a first approximation, $k_\lambda \cong k \cong cost$ can be assumed.

Second, the chemico-osmotic efficiency, ω, for a (1:1) electrolyte (e.g. Na Cl or KCl) can be expressed as follows:

$$\omega = 1 + \frac{\bar{c}_{sk,0}}{2\Delta c_s e_m}\left[Z_2 - Z_1 - (2t_c - 1)\cdot ln\left(\frac{Z_2 + 2t_c - 1}{Z_1 + 2t_c - 1}\right)\right] \qquad (30)$$

where

$$Z_1 = \sqrt{1 + \left(2c_s' \cdot e_m / \bar{c}_{sk,0}\right)^2}, \quad Z_2 = \sqrt{1 + \left(2c_s'' \cdot e_m / \bar{c}_{sk,0}\right)^2} \qquad (31)$$

$$t_c = \frac{D_{0c}}{D_{0c} + D_{0a}}. \qquad (32)$$

and t_c is the cation transport number (-), D_{0c} is the cation free-solution diffusion coefficient (m^2/s), and D_{0a} is the anion free-solution diffusion coefficient (m^2/s).

Third, the salt permeability can be expressed as follows:

$$P_s = (1-\omega)nD_s^* = nD_\omega^* \qquad (33)$$

where: D_ω^* is the global effective osmotic diffusion coefficient and D_s^* is the effective diffusion coefficient of the salt (m^2/s), given by:

$$D_s^* = \tau_m \frac{(\nu_c + \nu_a)D_{0c}D_{0a}}{\nu_a D_{0c} + \nu_c D_{0a}} \qquad (34)$$

Note that when $\bar{c}_{sk,0} \to 0$, $\omega \to 0$ such that the flux Eqs. 23 and 24 reduce to the expressions of the basic advective-diffusive transport theory.

4.1 Preliminary comparison of experimental and theoretical results

The first part of the proposed theoretical model previously described has been validated using a first series of experimental results reported in Malusis and Shackelford (2002a,b), Malusis et al. (2013), Dominijanni et al. (2013) and Shackelford et al. (2016). The experimental results were obtained by carrying out basically two kinds of tests, viz. 1) osmotic swelling pressure tests and 2) chemico-osmotic diffusive tests, and by using bentonites from two different GCLs, whose basic characteristics are reported in Table 1. Potassium chloride (KCl) solutions at different concentrations were used by Malusis and Shackelford (2002a,b), Malusis et al. (2013) and Shackelford et al. (2016), whereas, Dominijanni et al. (2013) used a sodium chloride (NaCl) as the salt.

The osmotic swelling pressure tests, that were carried out by Dominijanni et al. (2013), used an apparatus consisting of a stainless steel oedometer cell, a NaCl solution supply tank placed above a pressure panel board, a displacement transducer connected to the cell top piston, which is used to measure the axial strains of the specimen, a load cell, and a data acquisition system. The sample is confined by a rigid cell, which allows access to the water through both porous stones. The cell is connected to a pressure panel board that allows the specimen to be back-pressured. The rigid piston above the upper porous stone is connected to the load cell, which measures the pressure that has to be applied in order to hinder the axial strain of the specimen.

The test procedure requires a known amount of dry material to be dusted inside the oedometer ring, the cell to be assembled, and a NaCl solution to be supplied. The specimen, which is characterized by an initial dry height of 5 mm, is allowed to swell to 10 mm. The piston is then blocked, the sample is back-pressurized, and the steady-state swelling pressure is recorded after a short transitional phase. Since the bentonite that is initially dusted inside the oedometer is dry, the pressure increases for a number of days during the hydration phase, and then the steady-state swelling pressure is reached when hydration has been completed.

The chemico-osmotic diffusive test apparatus used in all the aforementioned studies to measure the salt permeability, P_s, (also defined, in the related literature, as the product of global osmotic effective diffusion coefficient, D^*_ω, times the porosity, n) is described in detail in Malusis et al. (2001).

Table 1. Selected physical and chemical basic properties for GCLs bentonites tested by Malusis and Shackelford (2002a,b), Dominijanni et al. (2013) and Shackelford et al. (2016)

Type	Bentomat®	GeobentXP®
Liquid Limit, LL (%)	478	525
Plasticity Index, PI (%)	439	-
Specific Gravity, G_s	2.43-2.68	2.65
Principal Minerals (%):		
montmorillonite	71	98
mixed-layer illite/smectite	7	-
quartz	15	-
other	7	-
Cation Exchange Capacity, CEC (meq/100g)	47.7	105

The main components of the apparatus are the osmotic cell, the flow pump system and the pressure transducer, which is used to measure the differential pressure that develops across the specimen during the test.

The cell consists of a modified rigid-wall permeameter, in which the top piston and the bottom pedestal are equipped with three ports each, with two ports enabling the different solutions to circulate through the top (e.g. NaCl or KCl solution) and through the bottom (e.g. deionized water) porous stones, with the aim of establishing a constant concentration gradient across the specimen. The third port is installed in both the top piston and the bottom pedestal to allow the differential pressure across the specimen to be measured. The flow pump system, which consists of a dual-carriage syringe pump and two stainless steel accumulators (actuators), prevents any volumetric flux through the specimen by simultaneously injecting into and withdrawing from the porous stones the same volume of solution. In order to obtain this result, the syringes have to displace the liquids across the top and bottom of the specimen at the same rate. All the tests were performed according to the procedure proposed by Malusis et al. (2001), whereby a solution containing a known electrolyte concentration (KCl or NaCl) was circulated in the top porous stone, while deionized water was circulated in the bottom porous stone. The concentration difference across the specimen was maintained constant by continuously infusing the two liquids at the boundaries of the specimen.

The interpretation of the previously illustrated tests series is summarized in Table 2 in terms of the primary chemico-physical parameters that have been obtained and which can be used in order to properly evaluate the bentonite barrier performances including the osmotic effect (among others).

Moreover, based on the proposed theoretical model, both the osmotic swelling pressure, u_{sw}, and the chemico-osmotic efficiency, ω, depend, particularly at low concentration, c_s, on the solid skeleton electric charge $\overline{c}_{sk,0}$ through Equations (15) and (30). Therefore, by regressing the theoretical curves with the experimental data for both the swelling and chemico-osmotic efficiency tests reported by Dominijanni et al. (2013), an average value of $\overline{c}_{sk,0}$ equal to 0.09 M was determined. The obtained theoretical curves are reported in Figures 4 and 5, together with the experimental data. The resulting agreement between theoretical and experimental data is very good also considering that, through the calibration of only one average parameter (i.e. the solid skeleton electric charge, $\overline{c}_{sk,0}$), reliable interpretations of very different kinds of tests (i.e. swelling and chemo-osmotic diffusion), involving both stress-strain behaviour and transport phenomena that occur within very complex systems as bentonite minerals with related pore fluids and electrolytes in solution, were possible.

Nevertheless, the most significant experimental data for determining the fitting parameters of the theoretical functions are those at the lowest concentrations and at the highest osmotic swelling pressure and osmotic efficiency, because, at the highest concentrations, both of the aforementioned properties tend to disappear regardless of the values of $\overline{c}_{sk,0}$ and, consequently, $N_{l,AV}$.

For this reason, in Figure 5, the experimental data from Shackelford et al. (2016), characterized by high c_s and low ω, have been reported together with the range of $N_{l,AV}$ values used for obtaining each experimental result from the lowest to the highest concentration values. For completeness, the corresponding $N_{l,AV}$ range has also been reported for the experimental data by Dominijanni et al. (2013).

In summary, the role played by the average number of lamellae per tactoid, in terms of osmotic swelling pressure and osmotic efficiency is increasingly reduced when the salt concentration of the external solution, c_s, increases and the osmotic efficiency, $\omega \rightarrow 0$.

Table 2. Properties of GCLs bentonites derived from the interpretation of Malusis and Shackelford (2002a,b) (a), Dominijanni et al. (2013) (b) and Shackelford et al. (2016) (a)

	(a)	(b)
Hydraulic Conductivity, k (m/s)	$9.00 \cdot 10^{-12}$ $1.63 \cdot 10^{-11}$	$8.00 \cdot 10^{-12}$
Porosity, n (-)	0.79	0.81
Void Ratio, e (-)	3.76	4.26
Effective Diffusion Coefficient, D^*_s (m^2/s)	$1.5 \cdot 10^{-10}$ $2.7 \cdot 10^{-10}$	$5.0 \cdot 10^{-10}$
Thickness, L (mm)	8 10	17
Average solid skeleton electric charge concentration, $\overline{c}_{sk,0}$ (M)	0.033 0.015	0.090

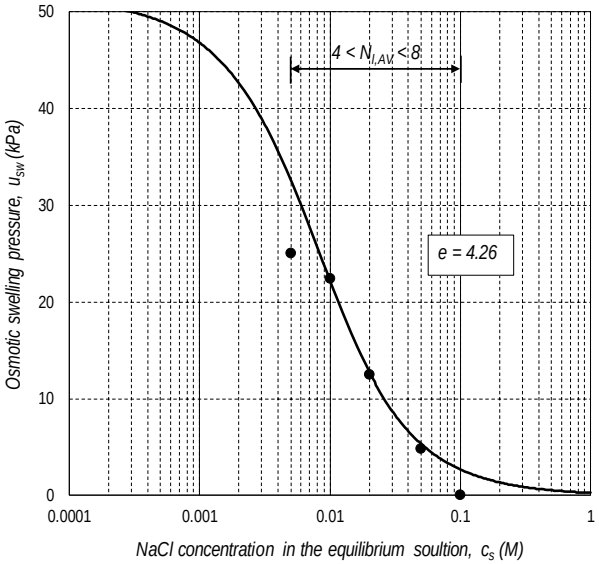

Figure 4. Osmotic swelling pressure as a function of salt equilibrium concentration with best-fitting theoretical curve.

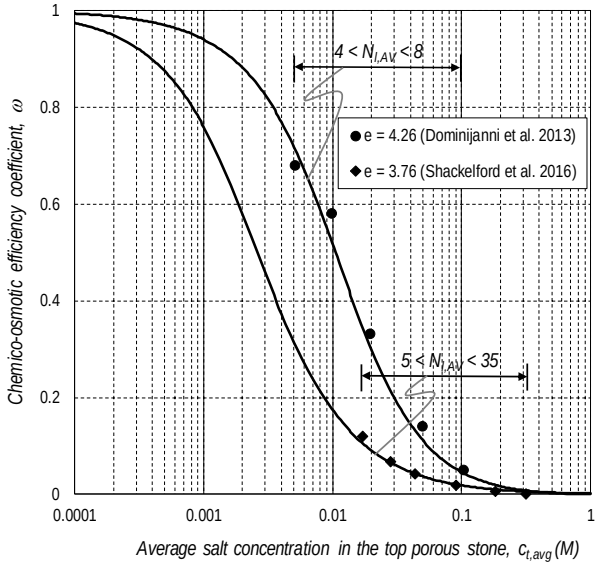

Figure 5. Chemico-osmotic efficiency coefficient as a function of the average salt concentration at top boundary of bentonite specimen with best-fitting theoretical curve (data from Dominijanni et al., 2013 and Shackelford et al., 2016).

However, other factors also may contribute to the differences in the diffusive behaviour of the two bentonites illustrated in Figure 5, such as different void ratio, differences in the original (natural) salt content of the bentonite samples and differences in which the specimens were prepared for testing.

A further and significant validation of the proposed theoretical approach, in terms of osmotic efficiency, is given by the complete set of the experimental data from the aforementioned studies as plotted in Figure 6. In this case, the theoretical linear relation from equation (33) is in very good agreement with the large number of experimental results.

This excellent result can be considered another important indication of the ability of the proposed theoretical approach to properly simulate the behaviour of bentonite systems in terms of osmotic efficiency.

In order to extend the assessment of bentonites performance to a range of higher salt concentrations, ($200 < c_s < 5000$ mM), and lower void ratios, ($0 < e < 2$) a second series of results from different experimental studies that provide for more significant variation in bentonite fabric, have been considered (see Table 3 and 4) and, via the interpretation of hydraulic conductivity, oedometer and swelling tests, the previously defined fabric state parameters ($N_{l,AV}$, S_{eff} and $\overline{c}_{sk,0}$) have been assessed.

In the case of the high ion concentrations, the fabric of the bentonites undergoes major changes due to flocculation particularly under low confining stress (i.e. high void ratio), resulting in a significant increase in the average number of platelets per tactoid and a correspondent decrease in the effective specific surface and fixed charge concentration of the solid skeleton (see Table 5).

In contrast, at very low ion concentrations but under very high confining stress, the distance between the bentonite platelets decreases resulting in the prevalence of attractive forces (van der Waals) relative to the repulsive electrochemical forces due to the negative charges on the platelet surface, with a consequent increase in the average number of lamellae per tactoid.

A comparison of this second series of experimental results with the theoretical predictions was conducted with the following considerations:

- Referring to the hydraulic conductivity tests on different bentonites and permeant solutions, an assessment of the effective specific surface, S_{eff}, has been performed using Eq. 29 (Kozeny, 1927; Carman, 1956; Dominijanni et al., 2013), neglecting, as a first approximation, the electro-viscosity coefficient, μ_{ev},, and referring to a steric tortuosity factor, τ_m, in the range from 0.2 to 0.3.
- An evaluation of the average number of platelets per tactoid, $N_{l,AV}$, and $\overline{c}_{sk,0}$ via Eqs. 2a, b and 13, respectively, and the assessment of the theoretical results in terms of osmotic swelling pressure, u_{sw}, by Eq. (15) (Dominijanni et al., 2013) were performed. The comparisons of the obtained theoretical osmotic swelling pressure with the experimental swelling test results for the same bentonite samples are shown in Figure 7.
- An additional assessment of the reliability of the proposed theoretical model, with reference to Eq. 15, is shown in Figure 8, where swelling and oedometer test results on samples permeated or hydrated with deionized water and with low concentration solutions ($c_s \leq 10$ mM) are shown together with the theoretical trend in terms of osmotic swelling pressure versus micro void ratio.

The good correlations obtained from comparing the theoretical model with experimental results in terms of osmotic efficiency, hydraulic conductivity and osmotic swelling pressures has provided motivation to attempt to generalize the proposed framework as described subsequently.

5 THE FABRIC STATE PARAMETERS AND THE RELATED SURFACE

As described previously, and considering the fundamental aspects concerning the complex chemico-hydro-mechanical behaviour of bentonites, with particular reference to the use of bentonites as barriers for subsoil pollutant control, the fundamental role played by the fabric or structure of solid skeleton once chemico-hydro-mechanical equilibrium has been achieved can immediately be observed (Shackelford et al., 2000; Guyonnet et al., 2005; Bourg et al., 2006).

As far as the conceptual schemes and the possible evolution of the bentonite fabric under the previously described mechanical stress-strain and/or electrolyte solution concentration actions are concerned, it is possible to introduce a series of state parameters (i.e. $N_{l,AV}$, S_{eff}, $\overline{c}_{sk,0}$) within which the most fundamental, direct and clear one results to be the average number of platelets per tactoid, $N_{l,AV}$.

The $N_{l,AV}$ state parameter plays a leading role in the second part of the proposed theoretical approach, in which an attempt is made to link the average number of platelets per tactoid, $N_{l,AV}$, to another two state parameters that define the external electro-chemical and mechanical actions, i.e. the electrolyte concentration, c_s, and the micro void ratio, e_m. The latter parameter can be defined through the total void ratio, e, which is easy to assess via the currently available laboratory tests, and the nano or interlayer void ratio, e_n, which can be evaluated, as a function of $N_{l,AV}$, from Eq. 3, once b_n and d_{Stern} have been estimated with reference to their very limited ranges of variation, which have already been defined.

5.1 The average number of lamellae per tactoid

As already shown, the average number of platelets per tactoid, $N_{l,AV}$, is directly linked to the effective specific surface, S_{eff}, and the effective fixed charge concentration of the solid skeleton, $\overline{c}_{sk,0}$, through Eq. 2a and Eq. 13.

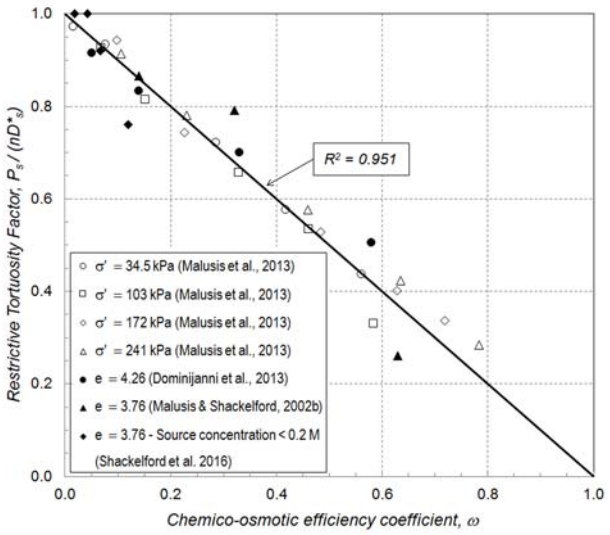

Figure 6. Restrictive tortuosity factor versus chemico-osmotic efficiency coefficient with the theoretical linear relation given by equation (33).

Table 3. Intrinsic Physical and Chemical Properties of the Considered Bentonites

Type	Dominijanni et al. (2013), Puma et al. (2015) and Boffa (2016)	Malusis and Shackelford (2002a,b)	Seiphoori (2014) and Manca (2015)	Mazzieri et al. (2011, 2013)	Di Emidio (2010)
Liquid Limit, *LL* (%)	525	478	420	530	650
Plasticity Index, *PI* (%)	-	439	355	480	600
Specific Gravity, G_s (-)	2.65	2.43	2.74	2.65	2.66
Principal Minerals (%):	98	71	85	90	95
montmorillonite	-	7	-	-	-
mixed-layer	-	15	4	-	-
illite/smectite	-	7	11	-	-
quartz					
other					
Cation Exchange Capacity, *CEC* (meq/100g)	105	47.7	74.0	94.5	44.5

Table 4. Range of the Physical and State Parameters of Bentonites in Contact with Deionized Water and NaCl, KCl and $CaCl_2$ Solutions

	Dominijanni et al. (2013) Puma et al. (2015) and Boffa (2016)	Malusis and Shackelford (2002a,b)	Seiphoori (2014)	Manca (2015)	Mazzieri et al. (2011, 2013)	Di Emidio (2010)
Hydraulic Conductivity, k (m/s)	$6.00\cdot10^{-12}$ $1.20\cdot10^{-10}$	$1.63\cdot10^{-11}$	$1.0\cdot10^{-14}$ $1.0\cdot10^{-13}$	$1.6\cdot10^{-11}$ $2.2\cdot10^{-8}$	$6.5\cdot10^{-11}$	$6.42\cdot10^{-12}$
Steric Tortuosity Factor, τ_m (-)	0.30 0.36	0.14	0.20	0.30 0.50	0.35	0.35
Total Void Ratio, e_{tot} (-)	0.60 4.50	3.76	0.53 1.20	2.15 5.40	5.13	2.55
Micro-Void Ratio, e_m (-)	0.10 2.99	2.56	0.05 0.38	1.23 4.35	3.6	1.13
Effective Diffusion Coefficient, D^*_s (m^2/s)	$5.0\cdot10^{-10}$	$2.7\cdot10^{-10}$	-	-	-	-
Osmotic Efficiency, ω (-)	0.00 0.68	0.35	-	-	-	-
Effective Specific Surface, S_{eff} (m^2/g)	24.14 216.71	164.40	36.18 92.15	6.09 121.81	159.65	129.94
Average Number of Platelets per Tactoid, N_{LAV} (-)	3.5 31.5	3.6	5.7 14.5	4.3 85.9	5.0	6.2
Stern Coefficient, f_{Stern} (-)	0.80 0.90	0.90	0.70	0.85	0.80	0,9
Fixed charge concentration, $\bar{c}_{sk,0}$ (M)	0.008 0.076	0.046	0.035 0.089	0.003 0.059	0.100	0.041

Table 5. Ranges of Variation of the Monovalent Ion Equivalent Concentrations that Influence the Main Performance Parameters of Bentonites at medium-to-high void ratios.

Main performance parameters of bentonite barriers	Range of monovalent ion concentration, c_s [mM]	Notes
Osmotic efficiency, ω	0 - 100	No fabric variation. For higher c_s than 100 mM $\omega = 0$
Osmotic swelling pressure, u_{sw}	0 - 200	Small fabric variation. For c_s around 200 mM $u_{sw} = 0$
Hydraulic conductivity, k	200 - 5000	Significant fabric variation and significant k increments
Steric tortuosity factor, τ_m	200 - 5000	Significant fabric variation and significant τ_m increments

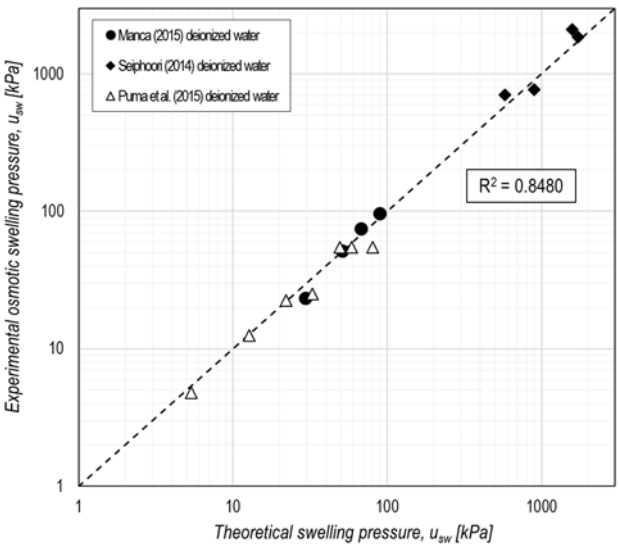

Figure 7. Experimental versus theoretical osmotic swelling pressure using input state parameters from hydraulic conductivity tests.

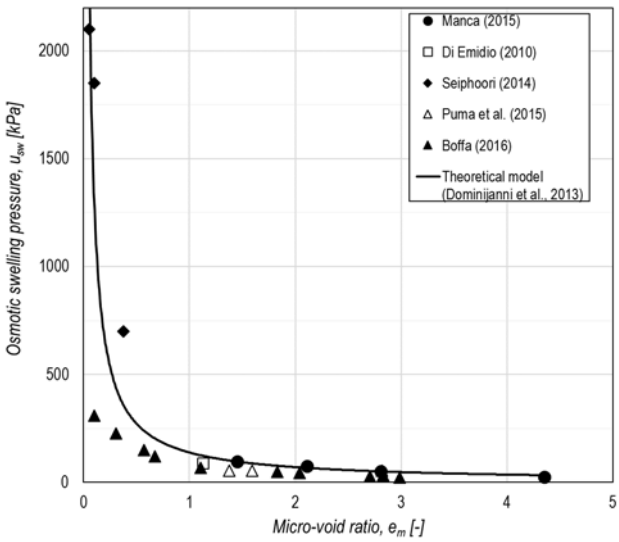

Figure 8. Osmotic swelling pressure versus micro-void ratio for samples tested with deionized water and solutions with a monovalent ion equivalent concentration $c_s \leq 10$ mM.

In particular, the effective specific surface, S_{eff} is inversely proportional to the average number of platelets per tactoid, N_{LAV} through the intrinsic parameter, S (=760 $m^2 \cdot g^{-1}$), i.e. the total specific surface of the single platelet.

Moreover, the effective fixed charge concentration, $\bar{c}_{sk,0}$, is also inversely proportional to N_{LAV} through the Faraday constant (F = 96,485 $C \cdot mol^{-1}$), a couple of intrinsic parameters, i.e. the unit electric surface charge of lamellae ($\sigma = 0.114$ C/m^2) and the density of the solid phase ($\rho_{sk} = 2.75$ g/m^3), and through a state parameter, i.e. the fraction of electric charge compensated by the cations specifically adsorbed in the Stern layer (-), f_{Stern}, which falls within a limited range ($0.70 < f_{Stern} < 0.95$). Therefore, this latter state parameter could, in the case, conveniently be used as a secondary fitting value to interpret a specific type of test conducted to investigate, for instance, the existence of still unproven or not precisely quantified kinds of flows, such as the hypothesised ionic diffusive surface flow (surface diffusion)

within very dense bentonites and/or the amount of cation exchange or sorption capacity during transient flow conditions (e.g., Glaus et al., 2007; Shackelford and Moore, 2013).

5.2 The fabric state surface (FSS)

As previously noted, the proposed state parameters are primarily influenced by the concentrations of ions, c_s, in the pore solution, and by the void ratio, which is in turn related to the effective isotropic component of the stress history of the considered bentonite.

Once the family of chemical state parameters that describe the bentonite fabric at the nano- and micro-scales have been defined, a parallel development can be formulated with some aspects in common with the well known elasto-plastic-work-hardening models of the traditional soil mechanics (e.g. the Cam Clay model) that are capable of describing the mechanical behavior of particulate media on the basis of a series of intrinsic and state parameters, as reported in Table 6.

As shown in detail in Dominijanni and Manassero (2012a,b) among others, the framework that includes the previously defined chemical parameters is able to link the coupled transport phenomena of water and ions by imposing chemical equilibrium between the bulk electrolyte solutions and the internal micro-pore solution at the macroscopic scale level, through the Donnan, Navier-Stokes and Nernst-Planck equations. In addition, some specific aspects of mechanical behaviour can be modelled and coupled to chemical and transport behaviour by taking into account different types of intergranular actions, apart from the solid contact stress and the bulk pore pressure (Terzaghi, 1943), such as electro-magnetic attraction/repulsion and osmotic swelling/suction forces (Mitchell and Soga, 2005).

In principle, and similar to the evolution of the basic Cam Clay model developed by Alonso et al. (1990) via the UPC model for unsaturated soil, the intrinsic and state parameters listed in Table 6 and the related framework can extend the basic theoretical approaches to include the mechanical behaviour that is related to the fabric of the active fine grained soils under fully saturated conditions, including not only actions such as the stress history and related void ratio, but also the ion species and concentration changes in the pore fluids.

In the following description, the developed framework is applied to interpret the whole data set from the aforementioned second series of experimental results taken from the literature and from the author's own laboratory tests, in order to illustrate the physico-chemico mechanisms that determine the observed macro-scale behaviour of active clays.

Finally, the basic state parameter, $N_{l,AV}$, has been assessed with reference to bentonite samples, which were in contact with both deionized water and chemical solutions including those at high concentrations. This parameter, which provides, as previously illustrated, a satisfactory prediction of the chemico-osmotic, hydraulic and swelling/shrinking behaviour of bentonites, is directly linked to the other two electro-fabric state parameters, i.e. S_{eff} and $\overline{c}_{sk,0}$.

Table 6: Intrinsic and State Parameters for Mechanical and Chemical Models

Fields	Actions	Intrinsic Parameters	State Parameters
Mechanical	Shear stress: τ	ρ_{sk}, φ_{cv}	e, p', ψ
Chemical	Ion concentration: c_s	S, σ	$N_{l,AV}$, S_{eff}, $\overline{c}_{sk,0}$, f_{Stern}, d_{Stern}

Notes: p'= isotropic effective stress component; ψ = dilatancy angle; φ_{cv} = friction angle at the critical state.

The resulting $N_{l,AV}$ values are plotted versus the micro-void ratio, e_m, in Figures 9 and 10, with Figure 10 simply being the enlargement of the vertical axis close to the origin of Figure 9.

In order to relate $N_{l,AV}$ to e_m and c_s, the following phenomenological equation is proposed:

$$N_{l,AV} = N_{l,AV0} + \frac{\alpha}{e_m} \cdot \left(\frac{c_s}{c_0} + 1 \right) + \beta \cdot e_m \cdot \left[1 - exp\left(-\frac{c_s}{c_0} \right) \right] \quad (35)$$

where c_0 represents the reference concentration (= 1 M), $N_{l,AV0}$ is the ideal average minimum number of lamellae per tactoid when $c_s = 0$ and $e_m \to \infty$; $\alpha = e_m \cdot \left(N_{l,AV} - N_{l,AV0} \right)$ for $c_s = 0$ is a coefficient relating $N_{l,AV}$ and e_m when $c_s = 0$ and β is a constriction coefficient that takes into account the limitation in movement of lamellae at medium-to-high void ratio due to mechanical constraints. The parameters $N_{l,AV0}$ and β both depend on the bentonite type, type of pre-treatments (e.g. removal of soluble salts, consolidation), hydration and chemical exposure sequence.

The micro-void ratio e_m in Eq. 35 can be derived from the total void ratio through the following equation:

$$e_m = \frac{e \cdot N_{l,AV} - S \rho_{sk} b_n \left(N_{l,AV} + d_d - 1 \right)}{N_{l,AV}} \quad (36)$$

Inserting Eq. 36 into Eq. 35 the number of lamellae per tactoid is related to the total void ratio and the salt concentration through a cubic equation, which can be solved analytically or numerically for given values of the parameters $N_{l,AV0}$, α, β, S, ρ_{sk}, b_n and d_d.

The available experimental data were regressed by imposing $N_{l,AV0}$ = 4.79, α = 0.91 and β = 42.45 (coefficient of determination, R^2 = 0.89).

Eq. 35 can be considered as an operative and simplified version of the formal theoretical equation reported in Figures 3a,b,c for medium-to-high void ratios. From Figures 3d,e,f, representing Eq. 35, very good agreement between the two surfaces is apparent, particularly with respect to the ascending branch versus the increasing micro void ratio. This good agreement can be considered as a further validation of the interpretation of the experimental data by the proposed simplified model through a formal and rigorous theoretical approach for medium-to-high e_m values.

Using this latter FSS equation for the proposed simplified model, it is now interesting to observe the regression results, in terms of average number of lamellae per tactoid, obtained from the interpretation of the aforementioned hydraulic conductivity and swelling tests belonging to the second series of experimental results.

The average number of lamellae per tactoid plotted versus the micro void ratio (i.e. the inter-tactoids void ratio) in particular shows, as expected, a very interesting trend.

In fact, for any given electrolyte concentration (apart from the unique case of deionized water), an initial decrease in $N_{l,AV}$ to a minimum value is followed by a continuous increasing trend with corresponding increase in the micro-void ratio.

More specifically, the ideal line, which represents the minimum loci of the aforementioned functions at the different ion concentrations, c_s, of the solutions in contact with the bentonite versus e_m may represent a separation locus between flocculating and dispersive behaviour of the considered bentonites, in a similar way to the case of unsaturated soils where swelling and shrinking behaviours are dependent on the degree of saturation (or suction) versus the confining stress and related void ratio (Alonso et al., 1990).

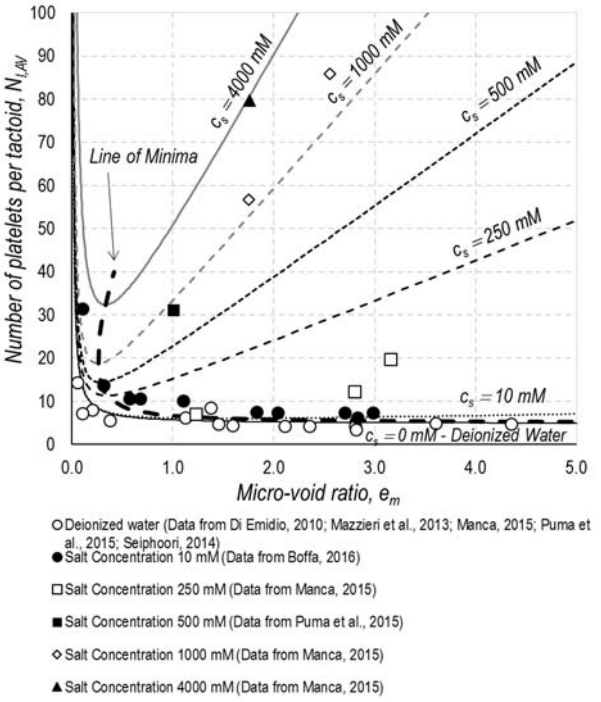

Figure 9. Average number of platelets per tactoid ($N_{l,AV}$) versus micro void ratio (e_m) based on values from the interpretation of hydraulic conductivity, osmotic and swelling tests (Fitting parameters: $N_{l,AV0} = 4.79$, $\alpha = 0.91$, $\beta = 42.45$; coefficient of determination, $R^2 = 0.89$).

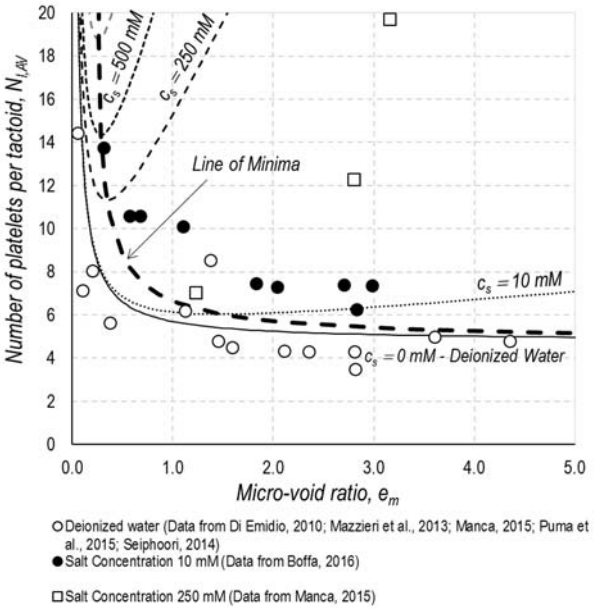

Figure 10. Enlargement of Fig. 9 for the range $0 < N_{l,AV} < 20$.

Some 3D views of the proposed FSS in the domain defined by the number of lamellae per tactoid, $N_{l,AV}$, the micro-void ratio, e_m, and the electrolyte concentration, c_s, are reported in Figure 11, together with the profiles defined by planar sections orthogonal to the main axes.

5.3 Determination of fabric state surface parameters

In order to determine the parameters of FSS, i.e. $N_{l,AV0}$, α, and β, for a specific bentonite, an experimental procedure, which minimizes the number of laboratory tests that have to be carried out, can be performed as follows.

First, two swelling tests at two different values of the total void ratio, e, are required to measure the osmotic swelling pressure in equilibrium with deionized water (i.e. with a solution having a null salt concentration, $c_s = 0$) under constant volume conditions. Since, on the basis of Eq. 15, the osmotic swelling pressure is a function of the micro-void ratio, e_m, and the number of lamellae per tactoid, $N_{l,AV}$, two values of $N_{l,AV}$ can be derived from the inversion of this relation, if an assumption on the values to be assigned to d_d and f_{Stern} is made. Once these two values of $N_{l,AV}$ have been obtained, the parameters $N_{l,AV0}$ and α can be calculated using the following equation:

$$\alpha = (N_{l,AV} - N_{l,AV0}) \cdot e_m \,, \tag{37}$$

which results from Eq. 35 for $c_s = 0$.

Second, a single hydraulic conductivity test is needed, using a permeant solution with a salt concentration, c_s, equal to the reference concentration, c_0 (= 1 M), to determine the value of $N_{l,AV}$ from the inversion of Eq. 29, by neglecting, as a first approximation, the electro-viscosity and assigning a value for the matrix tortuosity, τ_m. The parameter β can be obtained from this value of $N_{l,AV}$ through the following equation:

$$\beta = \left[\frac{exp(1)}{exp(1)-1} \right] \cdot \left[\frac{e_m \cdot (N_{l,AV} - N_{l,AV0}) - 2 \cdot \alpha}{e_m^2} \right] \tag{38}$$

which is derived from Eq. 35 for $c_s = c_0$.

If the tests for the aforementioned experimental procedure are not available, then the fabric state surface parameters can be estimated by implementing a best-fitting procedure on a set of data defined in the space of the variables $N_{l,AV}$, e_m, c_s, which are obtained from the interpretation of other laboratory test results. This last calibration method has been adopted for the estimation of the fabric state surface parameters that were described in section 5.2.

6 VALIDATION OF THE THEORETICAL MODEL

After the establishment of the last comprehensive version of the theoretical model introduced within the previous section, an additional validation was performed using a third series of experimental results reported in the literature and including direct and indirect measurements or assessments of the number of lamellae per tactoid versus micro void ratio and salt concentration in the external solution in equilibrium with the bentonite pore solution.

More specifically, in this last series of tests, particular attention has been given to the reliability of the model for the range of very reduced micro void ratio ($0 < e_m < 1$) consistent with the typical bentonite used in confinement systems for HLRW.

Moreover, the influence of the interaction with the geosynthetic fibers present in GCLs has also been considered, due to the increasing use of these products in modern landfill lining systems.

6.1 Experimental tests and results

Prior to illustrating and discussing the comparison of the experimental results with theoretical predictions, a summary of the primary features of direct and indirect tests and experimental techniques that have been used to determine the $N_{l,AV}$ values of the considered bentonites at different void ratios and salt solution concentrations is worthwhile.

This review also will illustrate the uncertainties and complexities associated with the estimation procedures for the average number of lamellae per tactoid of active clays and the expected reliability and precision of the different techniques.

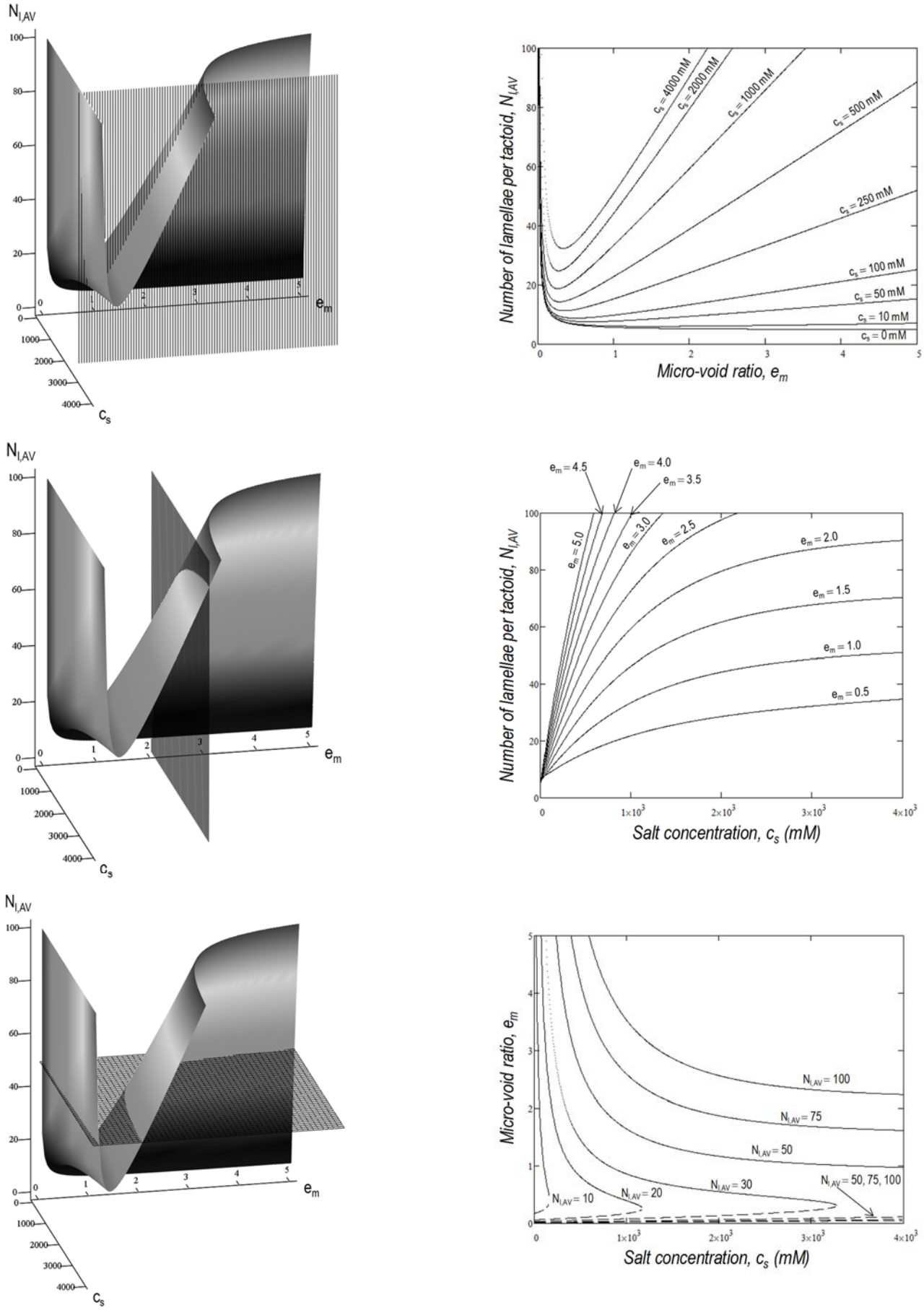

Figure 11. (a) 3D image of the fabric state surface (FSS); (b) planar section traces of the fabric state surface (FSS).

6.1.1 Direct methods

A number of experimental approaches, such as electron microscopies, spectroscopic analyses and diffraction techniques, have been employed for a direct assessment of the pore structure in compacted unsaturated and saturated bentonites, since the ratio of interlayer to non-interlayer water represents a key parameter governing water and solute transport.

Imaging techniques have been widely applied in order to observe bentonite microstructure (Laird et al., 1989; Tessier, 1990). Viola et al. (2005) have described the use of two innovative methods that are derived from traditional Scanning Electron Microscopy (SEM), viz., Field Emission Scanning Electron Microscopy (FESEM) that is equipped with a field emission electron emitter, which is brighter and therefore yields higher resolution than thermal emitters used in traditional SEM, and Environmental Scanning Electron Microscopy (ESEM) that offers the ability to observe porous materials under different hydration states without specific requirements for sample preparation.

FESEM micrographs can reach a magnification of 10000X, which allows the observation of the spatial arrangement of tactoids. Nevertheless, a limitation of the FESEM technique is associated with the sample preparation procedure, which requires a freezing process followed by ice transformation to vapour phase, in order to obtain a dried sample having a possibly preserved microstructure. In contrast, ESEM observations can be directly carried out on undisturbed hydrated samples in the microscope sample chamber. With this promising technique, the evolution of mesopores in sand bentonite mixtures can be observed during a dehydration process (Viola et al., 2005).

Furthermore, Transmission Electron Microscopy (TEM) is a high-resolution imaging technique that allows observation of the montmorillonite lamellae structure in compacted unsaturated and saturated bentonites over a wide range of magnifications (Matusewicz et al., 2013). TEM provides an observation of various microstructural features, such as nm-sized pores and the arrangement of dense tactoids of montmorillonite layers.

A limitation of all these imaging techniques is that the micrographs show only an extremely small portion of bentonite volume, thus having a limited representativeness, and cannot provide a quantification of the interlayer and non-interlayer pore volumes, or the average distance between the tactoids and between the lamellae inside the tactoids.

A common approach for the investigation of the interlayer pore space of montmorillonite is to apply X-ray diffraction (XRD) techniques to monitor interlayer expansion (Norrish, 1954). The XRD technique is based on the interaction of X-rays with atomic plane in the mineral crystalline structure. Reflections defining atomic plane spacings, mainly the basal spacing d_{001}, in combination with their integrated areas, become the primary criteria for mineral identification (Likos et al., 2010). However, the information provided by XRD analyses can be complicated by interstratification, because the combined effects of various basal spacings are not easily distinguished from those due to particle size, morphology, and orientation (Laird et al., 1989).

Muurinen et al. (2013) adopted Small Angle X-Ray Scattering Spectroscopy (SAXS) in order to study the changes in interlayer distances for bentonite samples. From these measurements, peak profile modelling was used to estimate the respective contributions of various mixed-layer structures to the observed peaks.

Although the diffraction techniques provide insight into alignment existing in stacked layers, they do not directly detect disordered complex non-interlayer geometries. In contrast, low field ^{1}H NMR is a reliable method for non-interlayer and interlayer volume characterisation and quantification (Manalo et al., 2003; Todoruk, 2003; Mitchell et al., 2008). The principle of the ^{1}H NMR relaxometry is to observe changes of the magnetisation owing to spin relaxation of protons back to equilibrium after excitation with an external static magnetic field. Spin relaxation is faster in the vicinity of solid surfaces, which is due to restriction of water mobility and interactions of protons with magnetic impurities along the pore wall, such as Mn^{2+} and Fe^{3+}. Since compacted saturated bentonites have a heterogeneous structure, pores are not isolated and NMR relaxation data are sums of exponentially decaying components, reflecting local surface-to-volume ratios. Experimental results may be turned into pore-size distributions by the so-called inversion of the decay data (Borgia et al., 1998).

NMR has previously been used successfully to determine the distribution of pore water in water-saturated bentonites (e.g., Ohkubo et al., 2008; Montavon et al., 2009; Muurinen et al., 2013; Ohkubo et al., 2016). Through an interpretation of the differences in observed proton mobilities, Montavon et al. (2009) were able to distinguish between three different populations, i.e. structural OH, external surface water and internal surface water. The problem of rapid exchange between external surface water and bulk water in water-saturated clays was solved by freezing samples to -25 °C. At this temperature, the bulk water was frozen and, thus, distinguishable from the surface water that was in a semi-liquid state.

In order to overcome the aforementioned lack of a clear differentiation of these types of water, Ohkubo et al. (2008) assumed that the relaxation time corresponding to a three-hydrated layer space may serve as a threshold to distinguish interlayer and non-interlayer water, whereas Ohkubo et al. (2016) adopted both the methodologies described above, and performed an investigation of the salt concentration effect of an NaCl solution on the pore-size distribution of compacted montmorillonite. By fitting discrete exponentials to the decay curves obtained from NMR measurements, Muurinen et al. (2013) found that the observed relaxation was composed of two major relaxation processes, and that assuming a third relaxation process produced a marginal effect. On the basis of these results, Muurinen et al. (2013) suggest the presence of only two water phases in water-saturated smectitic clays.

6.1.2 Indirect methods

Several indirect methods may be adopted in order to evaluate the microstructure of water-saturated bentonite and montmorillonite (i.e. how water is distributed between different pores in the clay fabric). These approaches are characterized by a common feature, since, in contrast to the direct methods, they require defining a structural model for the clayey soil, and the relationship existing between the primary state parameters and the macroscopic quantities which are measured by means of laboratory tests.

In light of the previously proposed theoretical framework, the osmotic efficiency ω in Eq. 30 is a function of the basic state parameter N_{LAV} through the fixed-charge concentration $\bar{c}_{sk,0}$. Thus, measurements of chemico-osmotic efficiency could be used to estimate the average number of lamellae per tactoid, and to predict the pore-water distribution on the basis of Eq. 3. Nonetheless, the osmotic efficiency disappears almost completely for high electrolyte concentrations (c_s > 100 mM), such that detecting the soil fabric changes in response to variations in the ionic strength of the equilibrium solution is not possible (e.g. Shackelford et al. 2016 found $0 < \omega < 0.02$ for $c_s \geq$ 100 mM).

A similar discussion pertains to the swelling pressure tests, given that the bentonite osmotic swelling pressure decreases to negligible values at high electrolyte concentrations (c_s > 200 mM). Moreover, the potentially significant uncertainty associated with laboratory tests performed to measure swell pressure should be recognized. For example, some studies conducted to measure the swell pressure of active clays have reported unexpectedly high values that are inconsistent with the specified boundary conditions (see e.g. Karnland et al., 2005).

The observed disagreement between the measured and predicted pressures can be attributed to the testing procedures, since in many cases a lack of attention is paid with respect to the complete dissipation of the suction component while hydrating the specimen.

Unlike the aforementioned macroscopic quantities, the hydraulic conductivity of smectitic clays undergoes significant changes as a result of different arrangements of the unit layers in the soil fabric, which influence in turn the micro-void space accessible for advective transport and the external specific surface. Therefore, hydraulic conductivity (permeability) tests represent an effective tool in order to investigate flocculation phenomena within a wide range of soil porosities and salt concentrations of the permeant solution. Additionally, according to Eq. 29 and neglecting the electro-viscous effect, the interpretation of hydraulic conductivity tests is independent of the assumption for the Stern fraction, f_{Stern}.

Apart from the aforementioned laboratory tests, other indirect experimental procedures have been found to be useful for the examination of the microstructure of active clays. For instance, the anion exclusion effect has recently been studied by means of different techniques. Van Loon et al. (2007) recognize that the diffusive behaviour of anions is a complex function of the electro-chemical interactions between the solutes and the porous medium. Indeed, in the case of negatively charged surfaces, anions are expelled from the diffuse double layer leading to a "negative adsorption" (Bolt and de Haan, 1982; Pusch et al., 1990), the extension of which depends on the composition of the equilibrium solution and the degree of compaction. The authors were able to estimate accessible porosities for chloride ions by interpreting the results of through-diffusion and out-diffusion tests performed on a Volclay KWK bentonite using the radionuclide $^{36}Cl^-$ as a non-sorbing tracer, and also by determining the concentration profile of stable Cl^-. In this latter case, upon completion of the out-diffusion test, the bentonite specimen was sliced in 1-mm-thick pieces, which were then dispersed in deionized water. Further details about these experimental procedures can be found in Molera et al. (2003), García-Gutiérrez et al. (2004), Muurinen et al. (2004), Muurinen et al. (2007), Birgersson and Karnland (2009), Tournassat and Appelo (2011), and Muurinen et al. (2013). Under the hypothesis of complete exclusion of anions from the interlayer space and from the Stern layer, which together represent the nano-void space, since anions are only partially repulsed from the larger pores of the interparticle space, the ion partition coefficient, Γ_2, given by Eq. 12, must be equal to the ratio of the anion accessible porosity, n^*, to the micro-void porosity, n_m. Thus, starting from this observation, it is possible to compute the value of the state parameter $N_{l,AV}$ and to derive the relative amounts of the different pore types.

6.2 Theoretical Predictions and comparison

The aforementioned third series of experimental results were used to validate the robustness of the model avoiding any further calibration of the fabric state surface (FSS) defining parameters.

First, results obtained through NMR measurements are analysed (Muurinen et al., 2013; Matusewicz et al., 2013; Ohkubo et al., 2016). The intrinsic properties and state parameters of bentonites tested through this method are reported in Table 7 and Table 8, respectively. This analysis of the soil microstructure can be considered as a direct method *sensu stricto*, because no assumptions need to be made with respect to the electro-chemical interactions which occur at the micro-scale, or with reference to the arrangement of unit layers. In fact, when the ratio of the interlayer to the non-interlayer pore-space is known, Eqs. 2 to 4 are sufficient to determine an average number of lamellae per tactoid.

As far as high void ratios are concerned, Figure 12 shows fairly good agreement between the considered experimental data and the proposed fabric state surface. In contrast, this agreement becomes poorer as the compaction degree increases.

The same conclusion is more effectively detailed in Figure 14. In order to obtain a reasonably good coefficient of determination, the data related to the lowest void ratios have to be omitted from the regression procedure.

A possible explanation of this observation can be obtained by taking into account the physical significance of the NMR results, since there is a risk of underestimating the non-interlayer porosity. In very high density samples, the difference between the average size of the interparticle pores and the interlamellar pores is not sufficiently large to discern the two pore types with this method (Järvinen et al., 2016). Thus, further study is recommended in order to improve the reliability of NMR for fine-grained soils, with a focus on evaluating to what extent the behaviour of the water contained inside the conductive pores is affected by magnetic interactions with the solid phase.

Muurinen et al. (2013) also performed SAXS measurements on the same Na-bentonite tested by NMR, and based on the measured basal distances, they were able to compute the amounts of interlayer water. Obviously, a similar computation requires the *a priori* definition of the internal specific surface (i.e. the state parameter $N_{l,AV}$), which was used by Muurinen et al. (2013) as a fitting parameter. Despite the uncertainty connected to this fitting approach, the interpretation of the literature data through the proposed fabric state surface can be considered satisfactory (Figure 12).

Table 7. Intrinsic Physical and Chemical Properties of Bentonites Determined Experimentally from Direct Methods

Type	Muurinen et al. (2013) and Matusewicz et al. (2013)	Ohkubo et al. (2016)
Specific Gravity of Solids, G_s (-)	2.75	2.80
Total Specific Surface (m^2/g)	610	760
Principal Minerals (%): montmorillonite	83.5	98.0
mixed-layer illite/smectite	0.7	-
quartz	2.8	-
other	-	-
Cation Exchange Capacity, CEC (meq/100g)	84.0	-

Table 8. Range of Physical and State Parameters of Bentonites Determined Experimentally from Direct Methods

	Muurinen et al. (2013)	Matusewicz et al. (2013)	Ohkubo et al. (2016)
Total Void Ratio, e_{tot} (-)	0.72 2.93	0.81 3.37	1.00 2.50
Micro-Void Ratio, e_m (-)	0.19 1.89	0.01 3.20	0.00 1.39
Effective Specific Surface, S_{eff}(m^2/g)	21.32 73.58	18.03 74.48	68.97 86.07
Average Number of Platelets per Tactoid, $N_{l,AV}$ (-)	8.3 28.6	8.2 33.8	8.8 11.0
Stern Coefficient, f_{Stern} (-)	0.85	0.85	0.85
Fixed charge concentration, $\bar{c}_{sk,0}$ (M)	0.010 0.036	0.009 0.036	0.034 0.043

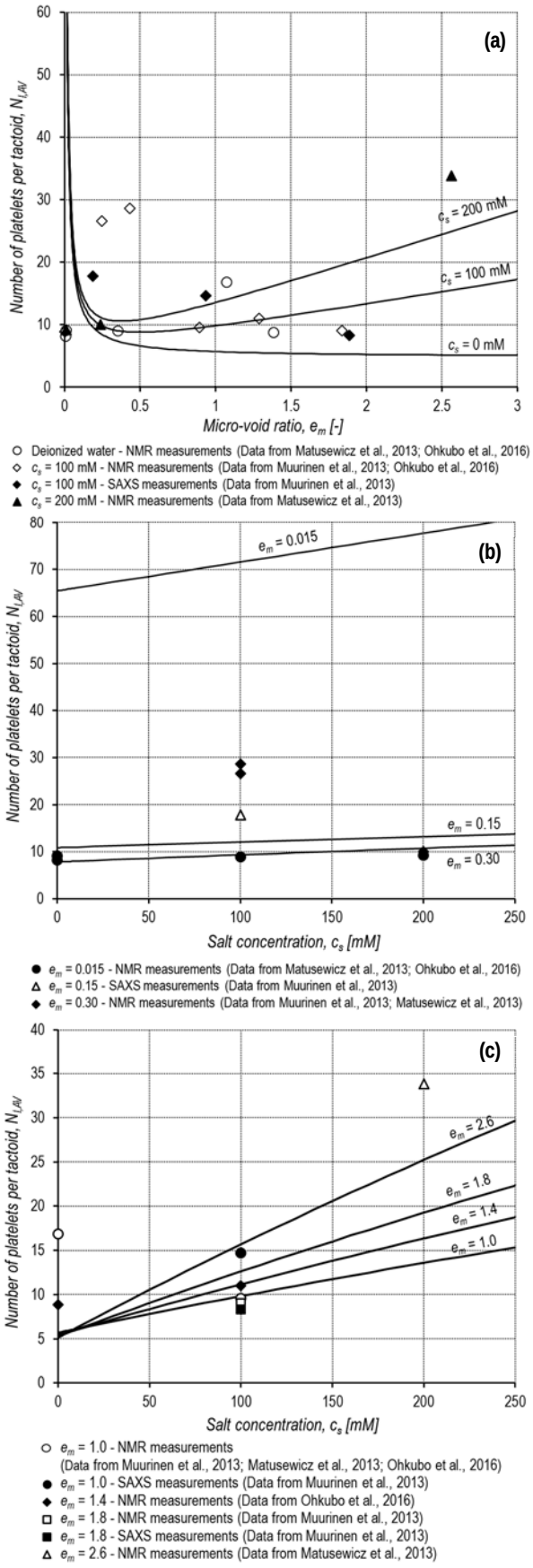

Figure 12. Comparison between the fabric state surface and experimental results taken from specialized literature (direct methods): (a) N_{LAV} vs e_m; (b) N_{LAV} vs c_s; (c) N_{LAV} vs c_s.

In Figure 13, experimental results obtained by the use of indirect methods are compared versus theoretical predictions. For this purpose, hydraulic conductivity (Jo et al., 2004; Lee and Shackelford, 2005; Katsumi et al., 2008; Shackelford et al., 2016; Ewy, 2017) and anion exclusion tests (Muurinen et al., 1989; Van Loon et al., 2007; Muurinen et al., 2013) are considered.

The intrinsic properties and the state parameters of bentonites tested through indirect methods (i.e. hydraulic conductivity tests and anion exclusion tests) are reported in Tables 9 through 12.

Table 9: Intrinsic Physical and Chemical Properties of Bentonites Determined Experimentally from Indirect Methods (Hydraulic Conductivity Tests)

Type	Jo et al. (2004)	Lee and Shackelford (2005) - LQB	Lee and Shackelford (2005) - HQB	Katsumi et al. (2008)	Shackelford et al. (2016)	Ewy (2017)	Petrov and Rowe (1997)
Liquid Limit, *LL* (%)	504	430	589	619.5	478	-	-
Plasticity Index, *PI* (%)	465	393	548	568.5	439	-	-
Specific Gravity, G_s of Solids(-)	2.65	2.74	2.78	2.839	2.68	2.70	2.61
Total Specific Surface (m^2/g)	620	540	790	880	650	250	750
Principal Minerals (%): montmorillonite	81.0	77.2	86.0	-	71.0	-	91.0
mixed-layer illite/smectite	-	-	-	-	7.0	46.0	-
quartz	-	3.4	3.5	-	15.0	20.0	5.0
other	-	-	-	-	7.0	-	-
Cation Exchange Capacity, *CEC* (meq/100g)	70.0	63.9	93.4	104.0	47.7	25.0 35.0	85.8

Table 10. Range of Physical and State Parameters of Bentonites Determined Experimentally from Indirect Methods (Hydraulic Conductivity Tests)

	Jo et al. (2004)	Lee and Shackelford (2005)	Katsumi et al. (2008)	Shackelford et al. (2016)	Ewy (2017)	Petrov and Rowe (1997)
Hydraulic Conductivity, *k* (m/s)	$5.1\cdot10^{-11}$ $1.9\cdot10^{-10}$	$7.0\cdot10^{-12}$ $2.4\cdot10^{-11}$	$5.8\cdot10^{-12}$ $2.2\cdot10^{-11}$	$9.0\cdot10^{-12}$	$2.9\cdot10^{-16}$ $7.4\cdot10^{-14}$	$4.8\cdot10^{-12}$ $2.9\cdot10^{-9}$
Steric Tortuosity Factor, τ_m (-)	-	-	-	0.092	-	-
Total Void Ratio, e_{tot} (-)	4.29 6.58	4.47 4.87	3.89 5.14	3.76	0.15 0.40	1.60 4.89
Micro-Void Ratio, e_m (-)	3.24 5.03	2.58 3.51	2.32 3.09	2.45	0.01 0.23	0.65 3.82
Effective Diffusion Coefficient, D^*_s (m^2/s)	-	-	-	$1.83\cdot10^{-10}$	-	-
Effective Specific Surface, S_{eff} (m^2/g)	64.61 196.51	186.54 240.67	116.88 339.28	146.60	3.50 28.41	16.17 123.08
Average Number of Platelets per Tactoid, N_{LAV} (-)	3.2 9.6	2.9 3.3	2.1 7.5	4.4	8.8 71.41	6.1 46.4
Stern Coefficient, f_{Stern} (-)	0.85	0.85	0.85	0.85	0.85	0.85
Fixed charge concentration, $\overline{c}_{sk;0}$ (M)	0.030 0.092	0.091 0.119	0.059 0.160	0.070	0.002 0.014	0.007 0.057

Table 11. Intrinsic Physical and Chemical Properties of Bentonites Determined Experimentally from Indirect Methods (Anion Exclusion Tests)

Type	Muurinen et al. (1989) and Muurinen et al. (2013)	Van Loon et al. (2007)
Liquid Limit, LL (%)	-	-
Plasticity Index, PI (%)	-	-
Specific Gravity, G_s (-)	2.75	2.80
Total Specific Surface (m^2/g)	610	560
Principal Minerals (%):		
montmorillonite	83.5	64.0
mixed-layer illite/smectite	0.7	7.0
quartz	2.8	4.0
other	-	-
Cation Exchange Capacity, CEC (meq/100g)	84.0	76.0 120.0

Table 12. Range of Physical and State Parameters of Bentonites Determined Experimentally from Indirect Methods (Anion Exclusion Tests)

	Muurinen et al. (1989)	Van Loon et al. (2007)	Muurinen et al. (2013)
Total Void Ratio, e_{tot} (-)	0.69 1.71	0.47 1.15	0.72 2.93
Micro-Void Ratio, e_m (-)	0.10 0.73	0.04 0.38	0.16 1.70
Effective Diffusion Coefficient, D^*_s (m^2/s)	-	-	-
Anion Accessible Porosity, n^* (-)	0.024 0.267	0.002 0.170	0.050 0.370
Effective Specific Surface, S_{eff}(m^2/g)	22.05 105.13	9.03 58.05	44.06 111.65
Average Number of Platelets per Tactoid, N_{LAV} (-)	5.9 28.2	9.6 62.0	5.4 13.8
Stern Coefficient, f_{Stern} (-)	0.85	0.85	0.85
Fixed charge concentration, $\bar{c}_{sk,0}$ (M)	0.011 0.051	0.004 0.029	0.021 0.054

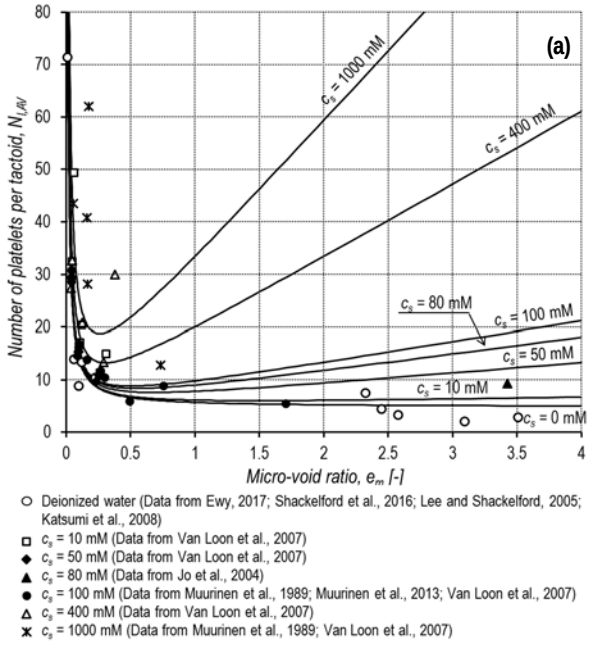

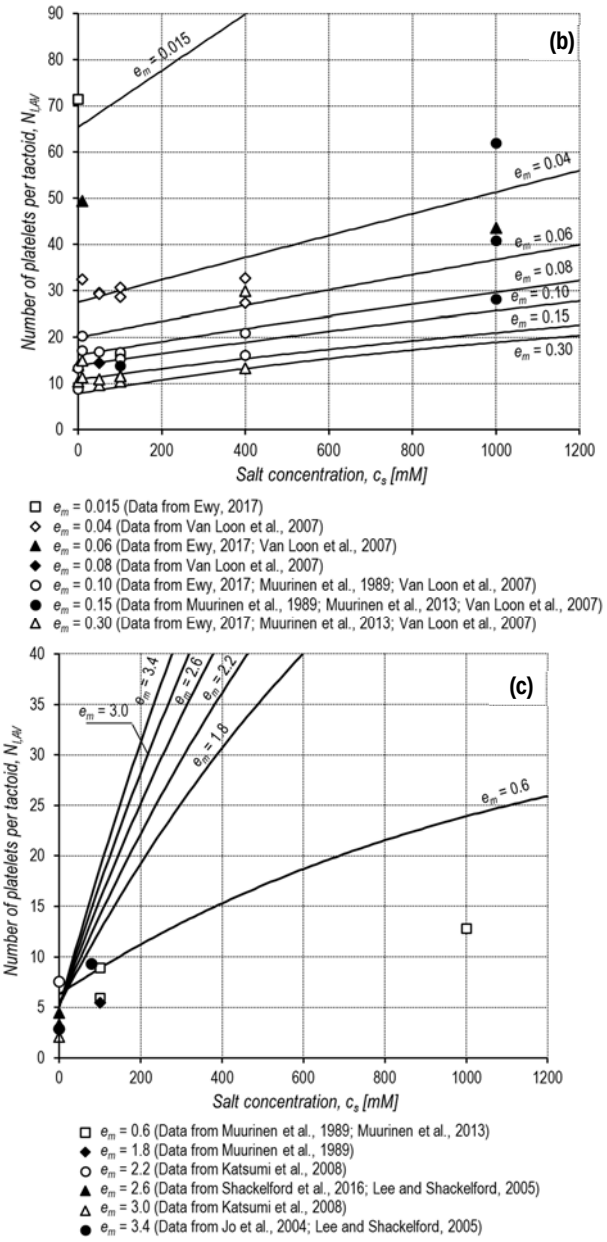

Figure 13. Comparison between the fabric state surface and experimental results taken from specialized literature (indirect methods): (a) N_{LAV} vs e_m; (b) N_{LAV} vs c_s; (c) N_{LAV} vs c_s.

Whereas data from Jo et al. (2004) and Ewy (2017) refer to a natural granular Na-bentonite and to shale samples, respectively, the other studies were based on permeability tests with deionized water on GCL specimens. Indeed, the hydraulic conductivity of GCLs can be affected by the needle-punching process. However, Puma et al. (2015) showed that the presence of needling across a GCL sample does not hinder swelling during hydration and does not influence the hydraulic conductivity of bentonites that are permeated by deionized water or dilute aqueous solutions. The agreement of the analysed literature data with the fabric state surface is good, and the scatter indicated in Figure 14 can be ascribed to the large variety of clay types considered in this study.

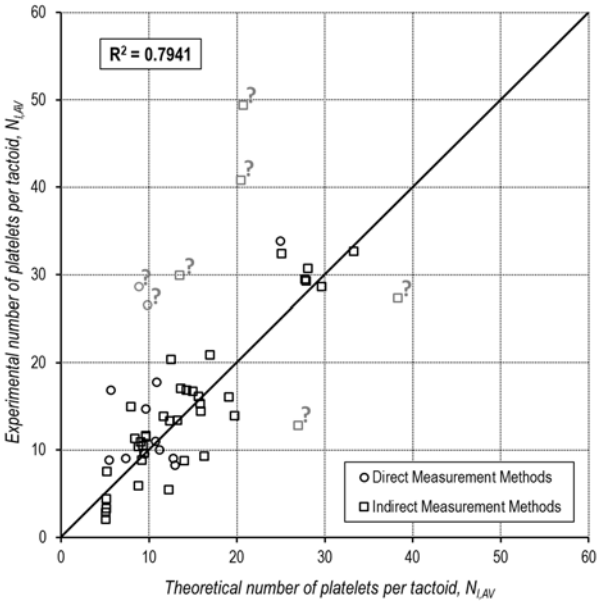

Figure 14. Experimental versus theoretical average number of lamellae per tactoid N_{LAV}, using literature data obtained through direct and indirect measurement methods (the grey points have not been used to compute the coefficient of determination).

Finally, an attempt was made to verify the possibility of adjusting the fabric parameters N_{LAV0}, α and β on a given set of tests results, related to the same clayey soil. As a matter of fact, all the elasto-plastic constitutive laws adopted for instance in traditional soil mechanics (e.g. Cam Clay model) must be calibrated on a restricted dataset pertaining to a specific clay. Accordingly, the parameters defining the proposed hydro-chemico-mechanical coupled model should also be differentiated for each tested clay, and the parameters specified in Section 5.2 can be used just as a rough approximation of the actual behaviour.

The experimental results provided by Petrov and Rowe (1997) were chosen for this analysis. The authors conducted hydraulic conductivity tests on a needle-punched GCL, subjected to pre-hydration with distilled water. The tests covered a wide range of effective confining stresses (from 3.4 to 114 kPa) and concentrations of the permeant NaCl solutions (from 0.01 to 2.0 M), thus providing a sizeable range of data available for calibration. The intrinsic properties and state parameters of the GCL tested by Petrov and Rowe (1997) are reported in Table 9 and Table 10, respectively. Incidentally, it has to be noted that, for this set of data, the interpretation via the same model parameters adjusted for natural bentonites may be incorrect conceptually, because of the potential impact resulting from the presence of the needle-punched fibres, which is expected to cause higher values of hydraulic conductivity due to the formation of preferential flow pathways along the fibres of the needling treatment when the GCL is permeated with solutions having a high salt concentration (Puma et al. 2015).

In Figure 15, the ordinary least squares has been applied for the data regression (N_{LAV0} = 1.56, α = 8.82, β = 10.01), and a high coefficient of determination has been obtained (R^2 = 0,9384) as shown in Figure 16. These results highlight the reliability of the simplified equation of the FSS, and its ability to simulate the coupled chemico-mechanical behaviour of active clays, once the fabric parameters have been properly assessed referring to the specific bentonite to be modelled.

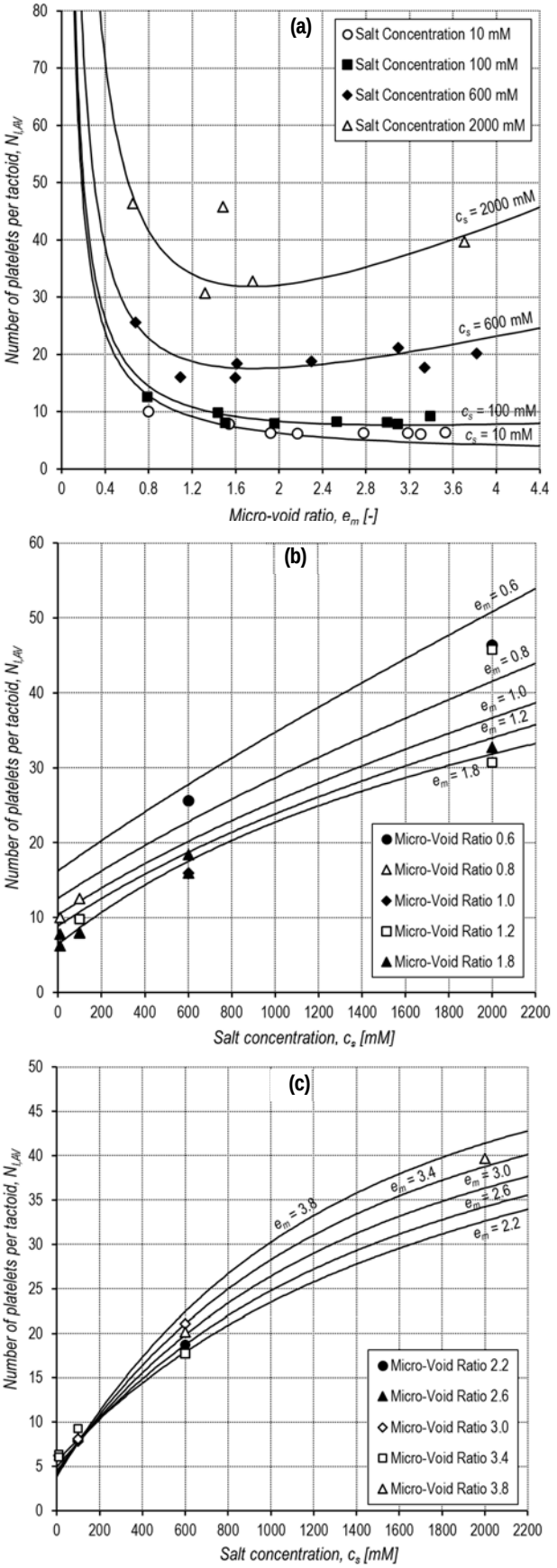

Figure 15. Calibration of the parameters that define the fabric state surface on the experimental results given by Petrov and Rowe (1997). (N_{LAV0} = 1.56, α = 8.82, β = 10.01) : (a) N_{LAV} vs e_m; (b) N_{LAV} vs c_s; (c) N_{LAV} vs c_s.

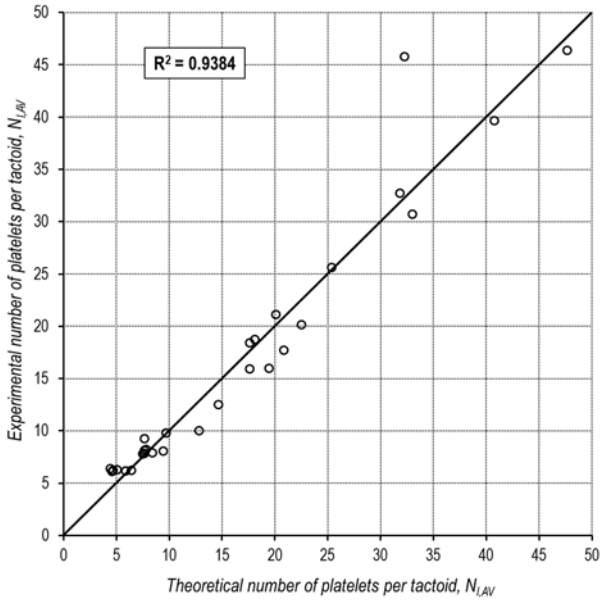

Figure 16. Experimental versus theoretical average number of lamellae per tactoid $N_{l,AV}$, using the hydraulic conductivity data provided by Petrov and Rowe (1997) and the related calibration of the fabric parameters.

8 CONCLUSION

Within the field of unsaturated soil mechanics, resistance and deformability of a given fine grained soil are governed primarily by two basic state parameters, i.e. void ratio and effective confining stress. Nevertheless, the degree of saturation and the related soil micro fabric or structrure also play an even more important role in detemining the mechanical behaviour of the considered fine grained soil (Alonso et al., 1990).

In a very similar way, the performances of a bentonite based barrier used for subsoil pollutant control, referring to fully saturated conditions, are governed, beyond density and confining effective stresses, by the ion valence and concentration of solutes in the pore solution and the related micro fabric or structure. In this case the barrier performances can be expressed in terms of hydraulic conductivity, diffusivity, osmotic efficiency and swelling properties (Manassero et al., 2016; Dominijanni et al., 2017).

Since bentonite particles can be considered as infinitely extended platy particles (platelets or lamellae), they can have a dispersed structure or fabric in which clay particles are present as well separated units, or as an aggregated structure that consists of packets of particles, or tactoids, within which several clay platelets are in a parallel array. The formation of tactoids has the net result of reducing the surface area of the montmorillonite, which then behaves like a much larger particle with the negative electrical charges being fully manifested on the outside surfaces and, therefore, the only charges capable of interacting with the mobile portion of the pore fluid and related ions in solution.

Referring to this very simple but fully realistic geometry, an effective fabric state parameter referred to as the average number of lamellae per tactoid, $N_{l,AV}$, has been defined. This fabric state parameter allows quantification in a very direct and clear manner of the micro fabric or structure of the considered bentonite. Moreover, $N_{l,AV}$ can be directly linked with the external or effective specific surface of the tactoids, S_{eff}, through the total specific surface of the single lamellae, S, and in turn with the average distances between tactoids and between the lamellae of the single tactoid together with the related micro, e_m, and nano, e_n, void ratios.

Referring to this framework, derivation of the other electrochemical parameters of the considered bentonite such as the effective solid charge concentration, $\bar{c}_{sk,0}$, the Stern fraction, f_{Stern}, and related Stern layer thickness, d_{Stern}, is possible.

Through the use of aforementioned state parameters coupled with the intrinsic parameters that characterize the solid phase of the considered bentonite, a theoretical model, capable of linking the coupled transport phenomena of water and ions by imposing the chemical equilibrium between the bulk electrolyte solutions and the internal micro-pore solution at the macroscopic scale level, through the Donnan, Navier-Stokes and Nernst-Planck equations, can be implemented. Moreover, the same model allows for the assessment of the osmotic component of the swelling pressure, u_{sw}, that, when introduced within the original effective stress principle of Terzaghi (1943), makes possible to define a general relationship among the micro void ratio, e_m, the electrolyte concentration, c_s and the average number of lamellae per tactoid for any given bentonite by simply taking into account the stress/strain equilibrium and compatibility within the porous medium. Within the 3-dimensional domain (e_m, c_s, $N_{l,AV}$), this relationship takes the shape of a surface referred to as the Fabric State Surface (FSS).

Owing to the complex mathematics of the aforementioned FSS derivation and related use, alongside the rigorous one, an approximate solution has been developed in order to generalize, and facilitate the application of the proposed model. The latter formulation has been used for the validation of the proposed framework and related theoretical models through the comparison of theoretical predictions, in terms of the average number of lamellae per tactoid, $N_{l,AV}$, with experimental results obtained from both direct (Nuclear Magnetic Resonance, X-ray diffraction, Small Angle X-ray Spectrometry, Transmission Electron Microscopy) and indirect (Hydraulic Conductivity, Swelling, Osmosis, Anion Available Pore Volume) experimental techniques.

The first two series of experimental results refer to six different sodium bentonites with smectite contents higher than 70%, which were used to define the three parameters that characterize the simplified version of the FSS, i.e. the ideal average minimum number of lamellae per tactoid, $N_{l,AV0}$, the coefficient α relating $N_{l,AV}$ and e_m when $c_s = 0$, and the constriction coefficient β that takes accounts for the possible movements of lamellae versus void ratio due to mechanical constrains. Moreover, a third series of tests with nine other sodium bentonites, but again with more than 64% of smectite content, was used for the final validation of the proposed theoretical model.

Before commenting on the obtained results, it is worth mentioning that the proposed FSS should, in principle, be defined for each bentonite type through a specific series of laboratory tests as described in section 5. Nevertheless, considering the relative similarity of the bentonites analysed within this paper, better fittings have been sacrificed for the greater statistical representativeness, that, today, can be obtained only from the greater number of experimental results that are available when all the aforementioned bentonites are considered together.

Apart from a small segment of the test results, that are suspect due to a series of uncertainties resulting from the questionable reliability of the experimental technique and related interpretation procedure, in particular, when reference is made to the specific parameter that we are looking for, the large majority of the experimental results are in a more than satisfactory agreement with the theoretical predictions, also considering the different experimental techniques (i.e. direct and indirect methods), the different kind of parameters to be assessed, the different laboratories and research groups and the different time periods associated with the considered test results.

When the parameters characterizing the FSS of a single bentonite and/or GCL, were determined on the basis of only tests conducted on the specific material, such as has been done in the case of the numerous series of hydraulic conductivity tests on a GCL from Petrov and Rowe (1997), the theoretical results predicted by the proposed model can be considered very good.

In summary, the proposed theoretical framework and related hydro-chemico-mechanical models seem to be able to estimate the performances of bentonite based barriers for subsoil pollutant control in terms of hydraulic conductivity, k, osmotic efficiency, ω, and osmotic swelling pressure, u_{sw}, once the intrinsic chemico-physical parameters, i.e., the solid phase density (ρ_{sk}), the total specific surface (S), and the fixed negative electric surface charge (σ) are known together with the following chemico-mechanical state parameters, i.e., the micro (e_m) and nano (e_n) void ratios, the average number of platelets or lamellae per tactoid ($N_{l,AV}$), the effective electric fixed-charge concentration ($\overline{c}_{sk0}$) and the Stern layer with reference to both its thickness (d_{Stern}) and fraction (f_{Stern}).

Nonetheless, a lot of work must still be done in the future in order to validate and, possibly, improve the aforementioned theoretical predictions together with the reliability of the experimental results.

Within these areas, two issues are worth noting in particular:

- From the experimental point of view, the improvement of the existing techniques and the implementation of new methods for bentonite nano and micro fabric determination are needed.
- From the point of view of the proposed theoretical model, a better definition of the roles played on the bentonite nano and micro fabric by both the stress/strain history and the electrolyte exposure history in terms of concentration and ions valence is needed.

Finally, extension of the theoretical framework and model to transition from fully saturated conditions to partially saturated conditions, is a more long term goal.

9 ACKNOWLEDGEMENTS

I would like to express my gratitude to the Members of the Technical Committee TC215 of ISSMGE for choosing the author to deliver the second R. Kerry Rowe Lecture, which is considered as one of the highest honors within the whole international geotechnical community. The author is also grateful to ENI S.p.A., Milan (Italy) for financing the research activity on bentonites carried out at the geotechnical laboratory of the Politecnico di Torino (Italy). Moreover, there are two colleagues, in particular, that actually make possible this work. They are professors Andrea Dominijanni from Politecnico di Torino (Italy) and Charles D. Shackelford from Colorado State University (USA). Their direct cooperation, stimulating discussions and valuable support are deeply recognized and appreciated by the author. The author also wish to acknowledge and to thank for the assistance and support the people from Geotechnical-Engineering professional firm, Torino (Italy) and the colleagues of the geotechnical research groups of Politecnico di Torino (Italy), École Polytechnique Fédérale de Lausanne, (Switzerland) and Università Politecnica delle Marche, Ancona (Italy). Finally, a special thank to the former Ph.D. student, Giacomo Boffa and to the candidate Ph.D. graduate student, Nicolò Guarena. for the cooperation in the preparation and editing of this paper.

10 REFERENCES

Alonso E., Gens A. and Josa A. 1990. A constitutive model for partially saturated soils. *Géotechnique* 40 (3), 405-430.

Altmann S. 2008 Geochemical research: a key building block for nuclear waste disposal safety cases. *Journal of Contaminant Hydrology*, 102 (3-4), 174-179.

Altmann S., Tournassat C., Goutelard F., Parneix J.-C., Gimmi T. and Maes N. 2012. Diffusion-driven transport in clayrock formations. *Applied Geochemistry*, 27 (2), 463-478.

Andra 2005. *Référentiel du comportement des radionucléides et des toxiques chimiques d'un stockage dans le Callovo-Oxfordien jusqu'à l'Homme*. Dossier 2005 Argile. Agence Nationale pour la gestion des déchets radioactifs, Châtenay-Malabry, France.

Birgersson M., and Karnland O. 2009. Ion equilibrium between montmorillonite interlayer space and an external solution – Consequences for diffusional transport. *Geochimica et Cosmochimica Acta*, 73, 1908-1923.

Bock H., Dehandschutter B., Martin C. D., Mazurek M., De Haller A., Skoczylas F. and Davy C. 2010. *Self-sealing fractures in argillaceous formations in the context of geological disposal of radioactive waste*. Nuclear Energy Agency, Organisation for Economic Co-operation and Development.

Boffa G. 2016. Mechanical and transport phenomena in advanced pollutants containment systems. Ph.D. Thesis. Politecnico di Torino, Torino (Italy).

Bolt G.H. 1956. Physico-chemical analysis of the compressibility of pure clays. *Géotechnique*, 6, 86-93.

Bolt G.H. and de Haan F.A.M. 1982. Anion exclusion in soil. In: Bolt G.H. (Ed.), *Soil Chemistry: B. Physico-chemical Models*. Elsevier, Amsterdam.

Borgia G.C., Brown R.J.S. and Fantazzini P. 1998. Uniform-penalty inversion of multiexponential decay data. *Journal of Magnetic Resonance*, 132 (1), 65-77.

Bourg I.C., Sposito G. and Bourg A.C.M. 2006. Tracer diffusion in compacted, water-saturated bentonite. *Clays and Clay Minerals*, 54(3), 363-374.

Carman P.C. 1956. *Flow of gases through porous media*. Butterworths, London.

Delay J., Vinsot A., Krieguer J.-M., Rebours H. and Armand G. 2007. Making of the underground scientific experimental programme at the Meuse/Haute-Marne underground research laboratory, North Eastern France. *Physics and Chemistry of the Earth, Parts A/B/C*, 32 (1-7), 2-18.

Di Emidio G. 2010. *Hydraulic and chemico-osmotic performance of polymer treated clays*. Ph.D. Thesis. Ghent University, Ghent (Belgium).

Dominijanni A. and Manassero M. 2005. Modelling osmosis and solute transport through clay membrane barriers. *Waste Containment and Remediation* (ASCE Geotechnical Special Publication No. 47), Alshawabkleh A. et al. (Eds.), ASCE, Reston/VA.

Dominijanni A. and Manassero M. 2008. Modeling the compressibility and the hydraulic conductivity of geosynthetic clay liners. *Proceedings of The First Pan American Geosynthetics Conference & Exhibition*, March 2-5, 2008, Cancun, Mexico.

Dominijanni A. and Manassero M. 2012a. Modelling the swelling and osmotic properties of clay soils. Part I: The phenomenological approach. *International Journal of Engineering Science*, 51, 32-50.

Dominijanni A. and Manassero M. 2012b. Modelling the swelling and osmotic properties of clay soils. Part II: The physical approach. *International Journal of Engineering Science*, 51, 51-73.

Dominijanni A., Manassero M. and Puma S. 2013. Coupled chemical-hydraulic-mechanical behaviour of bentonites. *Géotechnique*, 63 (3), 191-205.

Dominijanni A., Manassero M., Boffa G. and Puma S. 2017. Intrinsic and state parameters governing the efficiency of bentonite barriers for contaminant control, *Proceedings of Advances in Laboratory Testing and Modelling of Soils and Shales (ATMSS)*, Ferrari A. and Laloui L. (Eds.), January 18-20, 2017, Villars-sur-Ollon, Switzerland, Springer, 45-56.

Dominijanni A., Manassero M., Vanni D. 2006. Micro/macro modeling of electrolyte transport through semipermeable bentonite layers. *Proceedings of the 5th International Congress on Environmental Geotechnics*, June 26-30, 2006, Cardiff, Wales (UK), Thomas H.R. (Ed.), Thomas Telford, London, Vol. II, 1123-1130.

Ewy R.T. 2017. Shale capillarity, osmotic suction and permeability, and solutions to practical testing issues. *Proceedings of Advances in Laboratory Testing and Modelling of Soils and Shales (ATMSS)*, Ferrari A. and Laloui L. (Eds.), January 18-20, 2017, Villars-sur-Ollon, Switzerland, Springer, 29-36.

García-Gutiérrez M., Cormenzana J.L., Missana T. and Mingarro M. 2004. Diffusion coefficients and accessible porosity for HTO and $^{36}Cl^-$ in compacted FEBEX bentonite. *Applied Clay Science*, 26, 65-73.

Glaus M.A., Baeyens B., Bradbury M.H., Jakob A., Van Loon L.R. and Yaroshchuk A. 2007. Diffusion of ^{22}Na and ^{85}Sr in montmorillonite: evidence of interlayer diffusion being the dominant pathway at high compaction. *Environmental Science and Technology*, 41 (2), 478-485.

Grim R.E. 1962. *Applied Clay Mineralogy*, McGraw–Hill, New York.

Guyonnet D., Gaucher E., Gaboriau H., Pons C.H., Clinard C., Norotte V. and Didier G. 2005. Geosynthetic clay liner interaction with leachate: correlation between permeability, microstructure and surface chemistry. *Journal of Geotechnical and Geoenvironmental Engineering*, 131 (6), 740-749.

Guyonnet D., Touze-Foltz N., Norotte V., Pothier C., Didier G., Gailhanou H., Blanc P. and Warmont F. 2009. Performance-based indicators for controlling geosynthetic clay liners in landfill applications. *Geotextiles and Geomembranes*, 27 (5), 321-331.

Ichikawa Y., Kawamura K., Fujii N. and Kitayama K. 2004. Microstructure and micro/macro-diffusion behavior of tritium in bentonite. *Applied Clay Science*, 26, 75-90.

Järvinen J., Matusewicz M. and Itälä A. 2016. Methodology for studying the composition of non-interlamellar pore water in compacted bentonite. *Clay Minerals*, 51, 173-187.

Jo H., Benson C. and Edil T. 2004. Hydraulic conductivity and cation exchange capacity in non-prehydrated and prehydrated bentonite permeated with weak inorganic salt solutions. *Clays and clay minerals*, 52 (6), 661-679.

Kaczmarek M. and Hueckel T. 1998. Chemo-mechanical consolidation of clays: analytical solutions for a linearized one-dimensional problem. *Transport in Porous Media*, 32 (1), 49-74.

Karnland O., Muurinen A. and Karlsson F. 2005. Bentonite swelling pressure in NaCl solutions – Experimentally determined data and model calculations. *Proceedings of Advances in Understanding Engineered Clay Barriers*, November 12-14, 2003, Barcelona, Spain, Alonso E. and Ledesma A. (Eds.), Taylor & Francis Group, 241-256.

Katchalsky A. and Curran P.F. 1965. *Nonequilibrium thermodynamics in biophysics*. Harvard University Press, Cambridge, MA, USA.

Kato H., Muroi M., Yamada N., Ishida H. and Sato H. 1995. Estimation of effective diffusivity in compacted bentonite. In: Murakami T. and Ewing R.C. (Eds.), *Scientific Basis for Nuclear Waste Management XVIII*, Materials Research Society, Pittsburgh, Pennsylvania, 277-284.

Katsumi T., Ishimori H., Onikata M. and Fukagawa R. 2008. Long-term barrier performance of modified bentonite materials against sodium and calcium permeant solutions. *Geotextiles and Geomembranes*, 26 (1), 14-30.

Kozeny J. 1927. Ueber kapillare Leitung des Wassers im Boden. *Sitzungsber Akad. Wiss.*, Wien, 136 (2a), 271-306.

Laird D.A. 2006. Influence of layer charge on swelling of smectites. *Applied Clay Science*, 34 (1-4), 74-87.

Laird D.A., Thompson, M.L. and Scott, A.D., 1989. Technique for transmission electron microscopy and X-ray powder diffraction analyses of the same clay mineral specimen. *Clays and Clay Minerals*, 37 (3), 280-282.

Lee J.M., Shackelford C.D. 2005. Impact of bentonite quality on hydraulic conductivity of geosynthetic clay Liners. *Journal of Geotechnical and Geoenvironmental Engineering*, 131 (1), 64-77.

Leroy P., Revil A. and Coelho D. 2006. Diffusion of ionic species in bentonite. *Journal of Colloid and Interface Science*, 296 (1), 248-255.

Likos W.J., Bowders J.J. and Gates W.P. 2010. Mineralogy and engineering properties of bentonite. In: Bouazza A. and Bowders J.J. (Eds.), *Geosynthetic clay liners for waste containment facilities*, CRC Press/Balkema, Taylor & Francis Group, London.

Malusis M., Kang J., Shackelford C. 2013. Influence of membrane behavior on solute diffusion through GCLs. *Proceedings of Coupled Phenomena in Environmental Geotechnics (CPEG)*, July 1-3, 2013, Torino, Italy, Manassero M. et al. (Eds.), CRC Press/Balkema, Taylor & Francis Group, London, 267-274.

Malusis M.A. and Shackelford C.D. 2002a. Chemico-osmotic efficiency of a geosynthetic clay liner. *Journal of Geotechnical and Geoenvironmental Engineering*, 128 (2), 97-106.

Malusis M.A. and Shackelford C.D. 2002b. Coupling effects during steady-state solute diffusion through a semipermeable clay membrane. *Environmental Science and Technology*, 36 (6), 1312-1319.

Malusis M.A., Shackelford C.D. and Olsen H.W. 2001. A laboratory apparatus to measure chemico-osmotic efficiency coefficients for clay soils. *Geotechnical Testing Journal*, 24 (3), 229-242.

Manalo F.P., Kantzas A. and Langford C.H. 2003. Soil wettability as determined from using low-field nuclear magnetic resonance. *Environmental Science and Technology*, 37 (12), 2701-2706.

Manassero M. and Dominijanni A. 2003. Modelling the osmosis effect on solute migration through porous media. *Géotechnique*, 53 (5), 481-492.

Manassero M. and Dominijanni A. 2010. Coupled modelling of swelling properties and electrolyte transport through geosynthetic clay liner, *Proceedings of the 6th International Congress on Environmental Geotechnics*, November 8-12, 2010, New Delhi, India, Datta M. et al. (Eds.), Tata McGraw Hill, New Delhi, Vol. 1: 260-271.

Manassero M., Dominijanni A., Fratalocchi E., Mazzieri F., Pasqualini E. and Boffa G. 2016. About the state parameters of active clays, In: Benson C.H. and Shachelford C.D. (Eds.), Geotechnical Special Publication no. 274, *Geoenvironmental Engineering: Honoring David E. Daniel*, ASCE, 99-110.

Manassero M., Dominijanni A., Musso G. and Puma S. 2014. Coupled phenomena in contaminant transport. *Proceedings of the 7th International Congress on Environmental Geotechnics*, November 10-14, 2014, Melbourne, Australia, Bouazza A. et al. (Eds.), Engineers Australia, 144-169.

Manca D. 2015. *Hydro-chemo-mechanical characterization of sand/bentonite mixtures, with focus on their water and gas transport properties*. Ph.D. Thesis. EPFL, Lausanne (Switzerland).

Matusewicz, M., Pirkkalainen K., Liljeström V., Suuronen J.P., Root A., Muurinen A., Serimaa R. and Olin M. 2013. Microstructural investigation of calcium montmorillonite. *Clay Minerals*, 48 (2), 267-276.

Mazzieri F. and Di Emidio G. 2011. Caratteristiche e prestazioni di geocompositi bentonitici preidratati, *Proceeding of the 24th Italian Geotechnical Conference*, June 22-24, 2011, Napoli, Italy, AGI, Rome, 735-742 (in Italian).

Mazzieri F., Di Emidio G., Fratalocchi E., Di Sante M. and Pasqualini E. 2013. Permeation of two GCLs with an acidic metal-rich synthetic leachate. *Geotextiles and Geomembranes*, 40 (10), 1-11.

Mitchell J., Webber J.B.W. and Strange J.H. 2008. Nuclear magnetic resonance cryoporometry. *Physics Reports*, 461 (1), 1-36.

Mitchell J.K. and Soga K. 2005. *Fundamentals of soil behavior (3rd Edition)*. John Wiley and Sons, New York.

Molera M., Eriksen T. and Jansson M. 2003. Anion diffusion pathways in bentonite clay compacted to different dry densities. *Applied Clay Science*, 23, 69-76.

Montavon G., Guo Z., Tournassat C., Grambow B. and Le Botlan D. 2009. Porosities accessible to HTO and iodide on water-saturated compacted clay materials and relation with the forms of water: A low field proton NMR study. *Geochimica et Cosmochimica Acta*, 73 (24), 7290-7302.

Muurinen A., Carlsson T. and Root A. 2013. Bentonite pore distribution based on SAXS, chloride exclusion and NMR studies. *Clay Minerals*, 48 (2), 251-266.

Muurinen A., Karnland O. and Lehikoinen J. 2004. Ion concentration caused by an external solution into the porewater of compacted bentonite. *Physics and Chemistry of the Earth*, 29, 119-127.

Muurinen A., Karnland O. and Lehikoinen J. 2007. Effect of homogenization on the microstructure and exclusion of chloride in compacted bentonite. *Physics and Chemistry of the Earth*, 32, 485-490.

Muurinen A., Penttilä-Hilthunen P. and Uusheimo K. 1989. Diffusion of chloride and uranium in compacted sodium bentonite. In: *Scientific basis for nuclear waste management XII*, Lutze W. and Ewing R.C. (Eds.), Mater. Res. Soc. Symp. Proc. Materials Research Society, Pittsburgh, PA.

Norrish K. 1954. The swelling of montmorillonite. *Discussions of the Faraday Society*, 18, 120-134.

Ohkubo T., Ibaraki M., Tachi Y. and Iwadate Y. 2016. Pore distribution of water-saturated compacted clay using NMR relaxometry and freezing temperature depression; effects of density and salt concentration. *Applied Clay Science*, 123, 148-155.

Ohkubo T., Kikuchi H. and Yamaguchi M. 2008. An approach of NMR relaxometry for understanding water in saturated compacted bentonite. *Physics and Chemistry of the Earth*, 33, S169–S176.

Petrov R.J. and Rowe R.K. 1997. Geosynthetic clay liner (GCL) – chemical compatibility by hydraulic conductivity testing and factors

impacting its performance. *Canadian Geotechnical Journal*, 34, 863-885.

Puma S., Dominijanni A., Manassero M. and Zaninetta L. 2015. The role of physical pretreatments on the hydraulic conductivity of natural sodium bentonites. *Geotextiles and Geomembranes*, 43, 263-271.

Pusch R., Karnland O. and Hökmark H. 1990. *GMM – a general microstructural model for qualitative and quantitative studies of smectite clays*. SKB Technical Report 90-43, Swedish Nuclear Fuel and Waste Management Corporation, Stockholm, Sweden.

Seiphoori A. 2014. *Thermo-hydro-mechanical characterization and modelling of MX-80 granular bentonite*. Ph.D. Thesis. EPFL, Lausanne (Switzerland).

Shackelford C.D. and Moore S.M. 2013. Fickian diffusion of radionuclides for engineered containment barriers: diffusion coefficients, porosities, and complicating issues. *Engineering Geology*, 152, 133-147.

Shackelford C.D., Benson C.H., Katsumi T., Edil T.B. and Lin L. 2000. Evaluating the hydraulic conductivity of GCLs permeated with non-standard liquids. *Geotextiles and Geomembranes*, 18 (2-4), 133-161.

Shackelford C.D., Meier A. and Sample-Lord K. 2016. Limiting membrane and diffusion behavior of a geosynthetic clay liner. *Geotextiles and Geomembranes*, 44, 707-718.

Shainberg I., Bresler E. and Klausner Y. 1971. Studies on Na/Ca montmorillonite systems. 1. The swelling pressure. *Soil Science*, 111 (4), 214-219.

SKB 2011. *Long-term safety for the final repository for spent nuclear fuel at Forsmark*, SKB-TR-11-01, Svensk Kärnbränslehantering AB, Swedish Nuclear Fuel and Waste Management Co.

Skempton, A.W. 1961. Effective stress in soils, concrete and rocks. In: *Pore pressure and suction in soils*, Butterworths, London, 4-16.

Spiegler K.S. and Kedem O. 1966. Thermodynamics of hyperfiltration (reverse osmosis): criteria for efficient membranes. *Desalination*, 1 (4), 311-326.

Terzaghi K. 1936. The shearing resistance of saturated soil and the angle between the planes of shear, *Proceedings of 1st International SMFE Conference*, Harvard, Mass., Vol. 1, 54-56.

Terzaghi K. 1943. *Theoretical soil mechanics*, John Wiley and Sons, New York.

Tessier D. 1990. Behavior and microstructure of clay minerals. In: De Boodt M.F. et al. (Eds.), *Soil Colloids and their Associations in Aggregates*, Plenum Press, New York.

Tinnacher, R.M., Holmboe, M., Tournassat, C., Bourg, I.C. and Davis, J.A. 2016. Ion adsorption and diffusion in smectite: Molecular, pore, and continuum scale views. *Geochimica et Cosmochimica Acta*, 177, 130-149.

Todoruk T.R., Langford C.H. and Kantzas A. 2003. Pore-scale redistribution of water during wetting of air-dried soils as studied by low-field NMR relaxometry. *Environmental Science and Technology*, 37 (12), 2707-2713.

Tournassat C. and Appelo C.A.J. 2011. Modelling approaches for anion-exclusion in compacted Na-bentonite. *Geochimica et Cosmochimica Acta*, 75, 3698-3710.

Tournassat C., Chapron Y., Leroy P., Bizi M. and Boulahya F. 2009. Comparison of molecular dynamics simulations with triple layer and modified Gouy–Chapman models in a 0.1 M NaCl–montmorillonite system. *Journal of Colloid and Interface Science*, 339 (2), 533-541.

Van Loon L.R., Glaus M.A. and Müller W. 2007. Anion exclusion effects in compacted bentonites: towards a better understanding of anion diffusion. Applied Geochemistry, 22, 2536-2552.

Viola R., Tuller M., Or D. and Drasdis J. 2005. Microstructure of caly-sand mixtures at different hydration states. *Proceedings of Advanced Experimental Unsaturated Soil Mechanics (EXPERUS)*, June 27-29, 2005, Trento, Italy, Tarantino et al. (Eds.), Taylor & Francis Group, London, 437-442.

Yaroshchuk A.E. (1995). Osmosis and reverse osmosis in fine-charged diaphragms and membranes. *Advances in Colloid and Interface Science*, 60 (1-2), 1-93.